

CHAPTER IV

RESULTS AND DISCUSSION

4.1 The Effect of Operating Voltage to the Morphology of Synthesized Fibers

The inorganic hollow fibers were carried out using the combination of sol-gel method and electrospinning process to produce fibrous materials from the mixed solution of sol-gel precursors with polymer binder in organic solvent. The viscous polymer binder plays significant roles in building up the viscosity for fiber formation and in controlling the fibrous morphologies. In order to form continuous and uniform hollow fibers in the process, parameter related to the immiscibility of core and shell is the most important factor to be concerned. Thus, mineral oil was used as a core solution in this research. By applying various high operating voltages across the end of needle and the collector; fibers were spun toward the collector as a non-woven material. The SEM was utilized to examine the surface morphology of the obtained materials.

4.1.1 TiO₂ Hollow Fibers, Zn/TiO₂, and Ag/TiO₂ Composite Hollow Fibers

TiO₂ hollow fibers was prepare through the coaxial electrospinning process under the fixed condition of 17 cm working distance between a tip of the needle to the surface of the collector as aforementioned in the previous chapter. The influence of applied electrostatic field strength on the morphological appearances of pre-calcined fibers at 15, 17, 19, 21, 23, and 25 kV are shown in Figure 4.1 (a-f). Apparently, the morphological appearances of pre-calcined fibers at 15 kV showed the smooth, continuous and uniform fibers with the average diameter of $0.91 \pm 0.07 \mu\text{m}$ and a thickness of $70 \pm 5 \mu\text{m}$. In contrast to the others, the morphological appearances of pre-calcined fibers seemed to be non-uniform ejection of the jets with increasing operating voltages that may be the result of the changing in the electrostatic force which is responsible for the mass throughput of the solution. Normally, increasing in electrostatic strength causes a rise in both the electrostatic force and the Coulombic repulsion force. With increasing in electrostatic strength, the decreasing in the average diameter of the obtained fibers occurred as shown in Table 4.1. This evidence revealed an increase in the Coulombic repulsion force,

which was responsible for the stretching of ejection jets during the process, led to a decrease in the fiber diameters. Figure 4.2 shows the relationship between the diameters of pre-calcined TiO_2 hollow fibers and applied electrostatic potential and the error bars represent standard deviation of the average fiber diameter data.

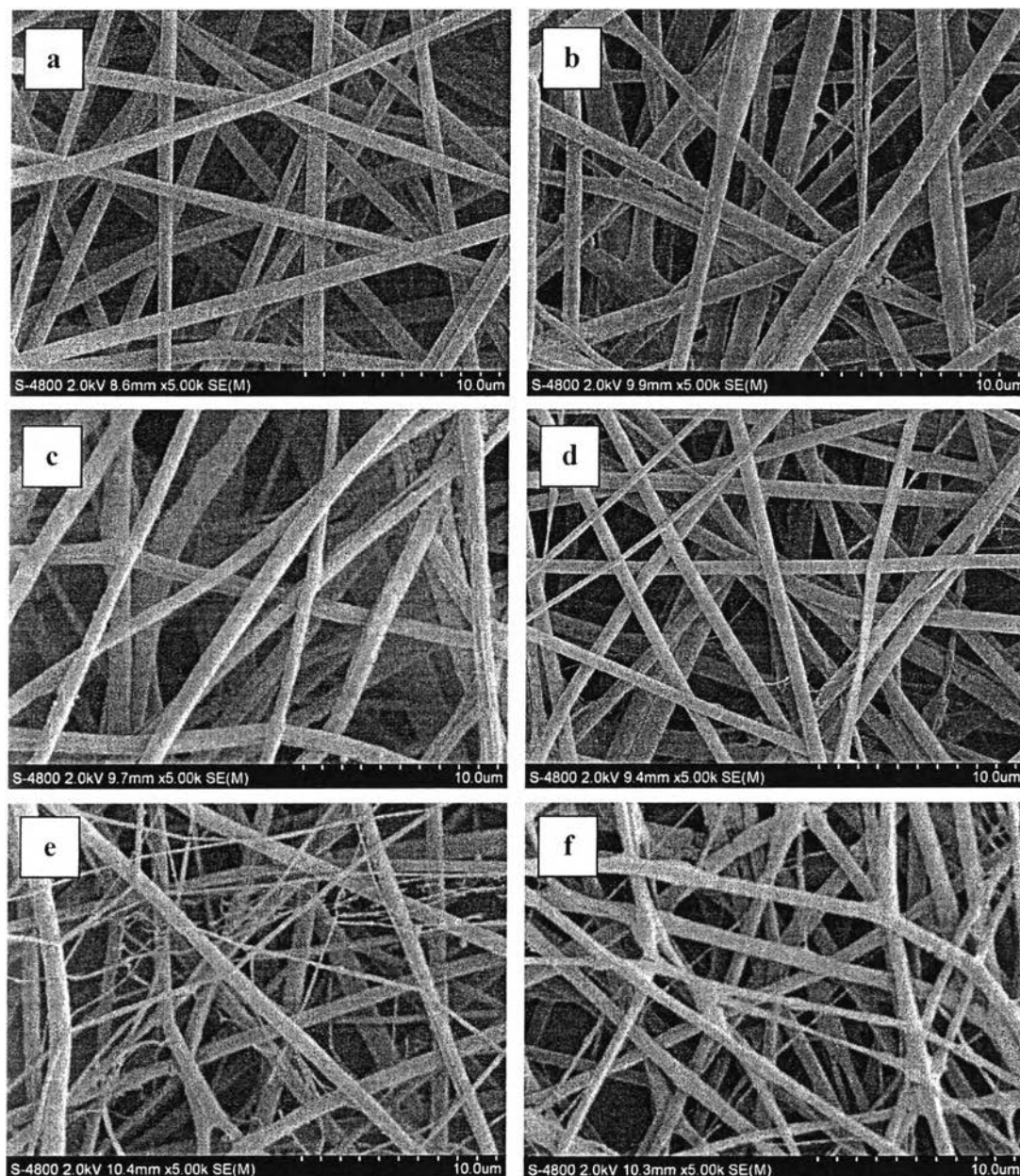


Figure 4.1 SEM images (magnification = 5000X; scale bar = 10.0 μm) of the pre-calcined TiO_2 hollow fibers under the fixed condition of 19 cm working distance at

operating voltage of (a) 15 kV, (b) 17 kV, (c) 19 kV, (d) 21 kV, (e) 23 kV, and (f) 25 kV.

Table 4.1 The average diameter of the pre-calcined TiO₂ hollow fibers

Working Distance (cm)	Operating Voltage (kV)	Average Diameter (μm)
17	15	0.91 ± 0.07
17	17	0.90 ± 0.15
17	19	0.85 ± 0.12
17	21	0.82 ± 0.07
17	23	0.81 ± 0.08
17	25	0.70 ± 0.12

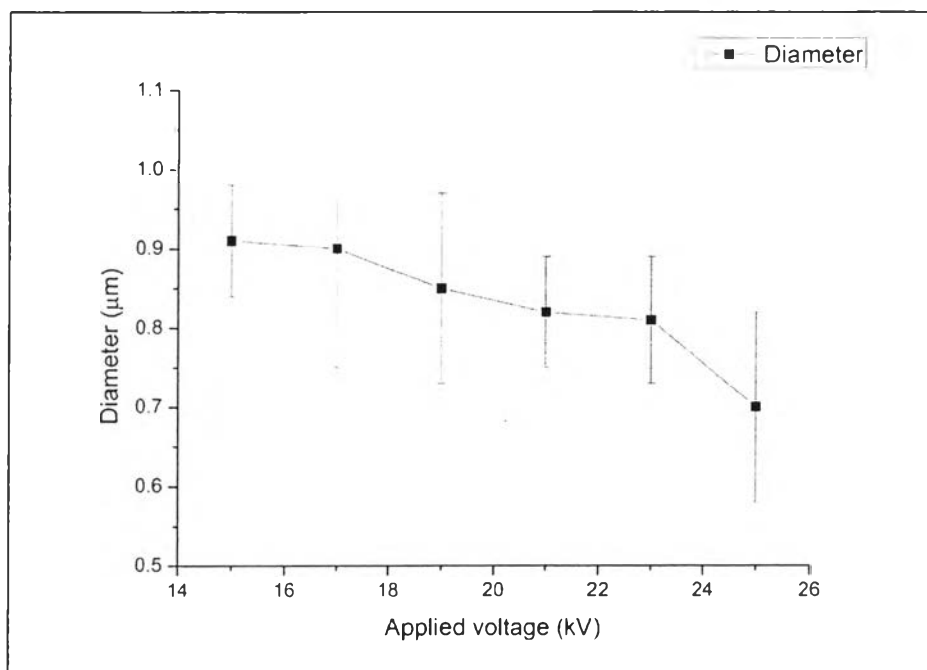


Figure 4.2 The average diameter of pre-calcined TiO₂ hollow fibers as a function of applied voltage (across a fixed working distance of 17 cm).

For pre-calcined Zn/TiO₂ and pre-calcined Ag/TiO₂ composite hollow fibers, they were also successfully produced via coaxial electrospinning process under the proper spinning condition of 15 kV operating voltage and 17 cm working distance. The fibrous materials with a thickness of $70 \pm 5 \mu\text{m}$ were obtained. As can be clearly seen in Figure 4.3 (a and b), uniform and continuous fibers were formed with the average diameter of $0.90 \pm 0.08 \mu\text{m}$ and $0.87 \pm 0.10 \mu\text{m}$ of pre-calcined Zn/TiO₂ and pre-calcined Ag/TiO₂ composite hollow fibers, respectively. These could be demonstrated the obtained morphologies of these two pre-calcined composite hollow fibers had not been affected by the addition of Zn and Ag powder in the spinning solution. They, however, had rougher surface compared to the pre-calcined TiO₂ hollow fibers when considering of the texture of each individual fiber. These results might be involved with the addition of Zn and Ag powders into spinning solution.

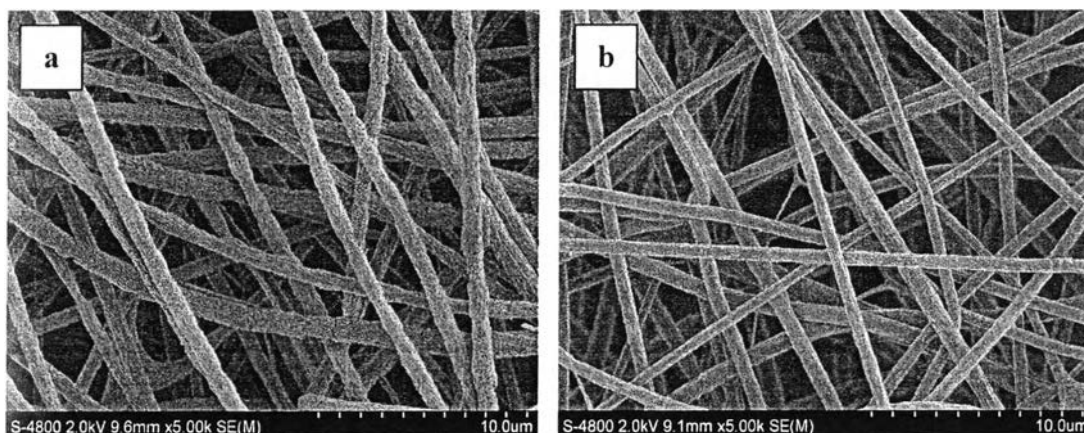


Figure 4.3 SEM images (magnification = 5000X; scale bar = 10.0 μm) of (a) pre-calcined Zn/TiO₂ and (b) pre-calcined Ag/TiO₂ composite hollow fibers under the proper electrospinning condition of 15 kV/17 cm.

4.1.2 TiO₂ Fibers

TiO₂ fibers were accomplished via the electrospinning process under the suitable spinning condition of 15 kV operating voltage and 17 cm working distance. The appearance in morphology showed the smooth texture with continuous

and uniform fibers (Figure 4.4). The average diameter and a thickness of the product obtained were also observed to be $0.91 \pm 0.06 \mu\text{m}$ and $70 \pm 5 \mu\text{m}$, respectively.

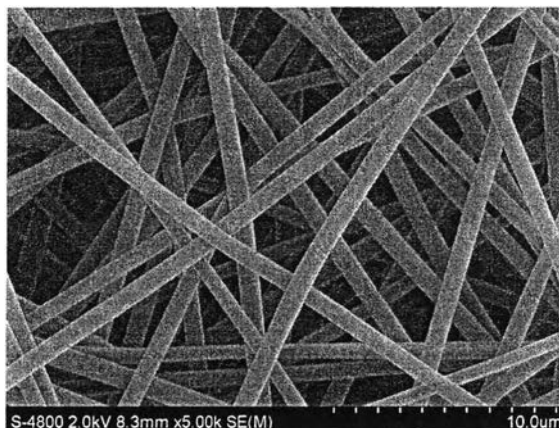


Figure 4.4 SEM images (magnification = 5000X; scale bar = 10.0 μm) of the pre-calcined TiO_2 fibers under the proper electrospinning condition of 15 kV/17 cm.

4.2 The Effect of Calcination Process to the Morphology and the Crystal Structure of Synthesized Fibers

4.2.1 Calcination Condition at Different Time and Temperature

After the electrospinning process under a fixed condition of 15 kV/17 cm, the pre-calcined TiO_2 hollow fibers were initially dried in the oven at 80 °C for 2 days to remove solvent and complete the hydrolysis. They were then calcined in air atmosphere with a heating rate of 5 °C minute^{-1} at 500 °C for 1,2,3 h, 600 °C for 1,2,3 h, and 650 °C for 1,2,3 h. The X-ray diffractometer (XRD) was used to determine the crystal structure of the synthesized fibers. Moreover, The SEM and TEM were utilized to investigate the surface morphology and structure of the obtained materials. The functional groups of the synthesized fibers can be determined by FTIR spectrum as well.

Fig 4.6 reveals the XRD pattern of calcined TiO_2 hollow fibers which were operated in air atmosphere with a heating rate of 5 °C minute^{-1} at different conditions. It is noteworthy that the fibers prior to calcination were amorphous (see Figure 4.5), meanwhile the calcined fibers occurred crystallization during the

calcination process. The anatase phase of crystalline TiO_2 has been obtained after the calcination process. All of calcination conditions provided pure anatase titania fibers without contamination of the other phases (JCPDS card No 21-1272) which furnished favorable crystal structure for lithium-ion insertion during charge-discharge process due to the most electroactive host. At room temperature, anatase structure can accommodate charge of 0.5-1 mole of lithium without any major structure change. However, in case of rutile and brookite, they are negligible at room temperature.

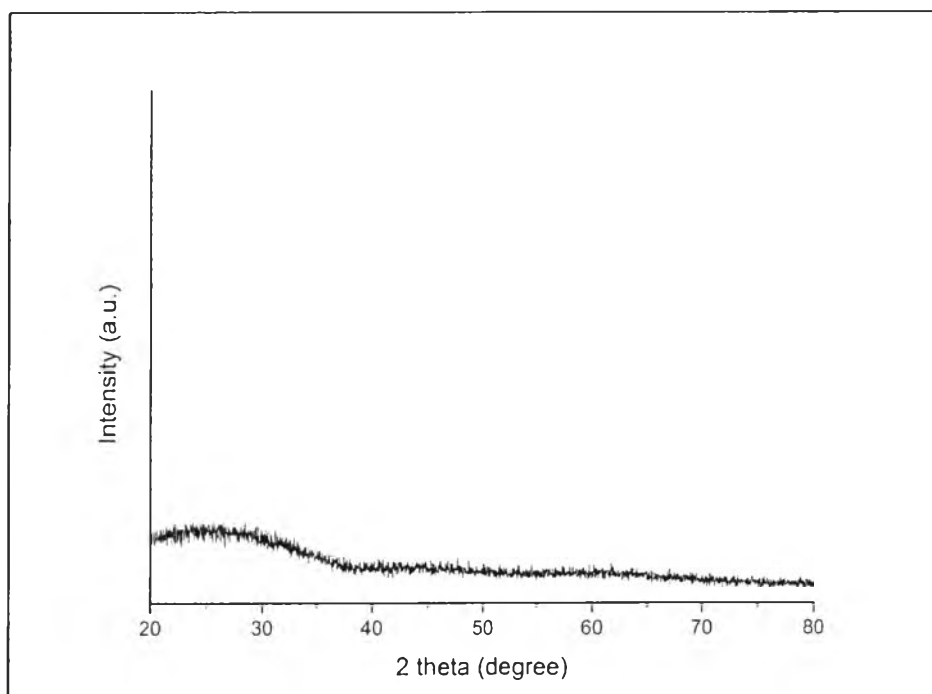


Figure 4.5 XRD results of TiO_2 hollow fibers before calcination.

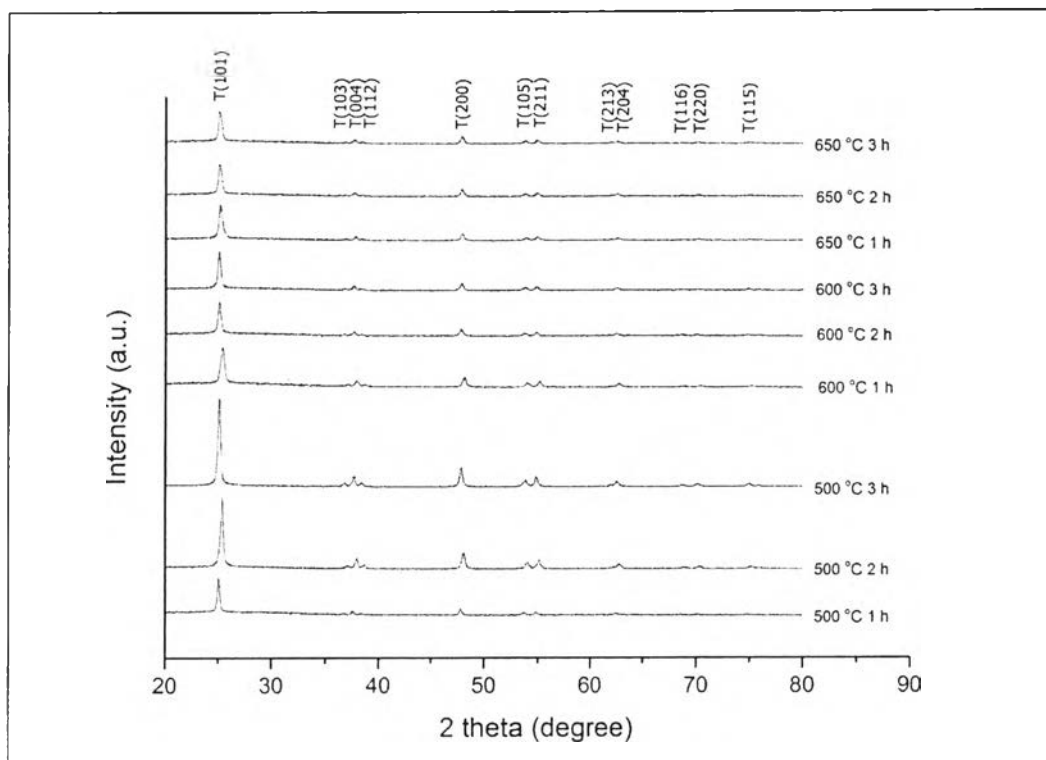


Figure 4.6 XRD results of TiO_2 hollow fibers at various calcination conditions.

The percentage of crystallinity was shown in Table 4.2. According to the results, at 500 °C, the percentage of crystallinity increased with increasing time of calcination, showing the improvement of crystallinity of anatase phase. But there are some noteworthy results at the calcination temperature of 600 °C and 650 °C. The longer the time of calcination, the lower percentage of crystallinity obtained. Moreover, a decreasing in crystallinity tended towards the higher calcination temperatures. The details of crystallite size were calculated from the Scherrer's equation and also displayed in Table 4.3. According to the results, in each temperature, the crystallite size increased as the time increased. In case of temperature, the crystallite size tended to increase as a function of the temperature.

Table 4.2 The percentage of crystallinity

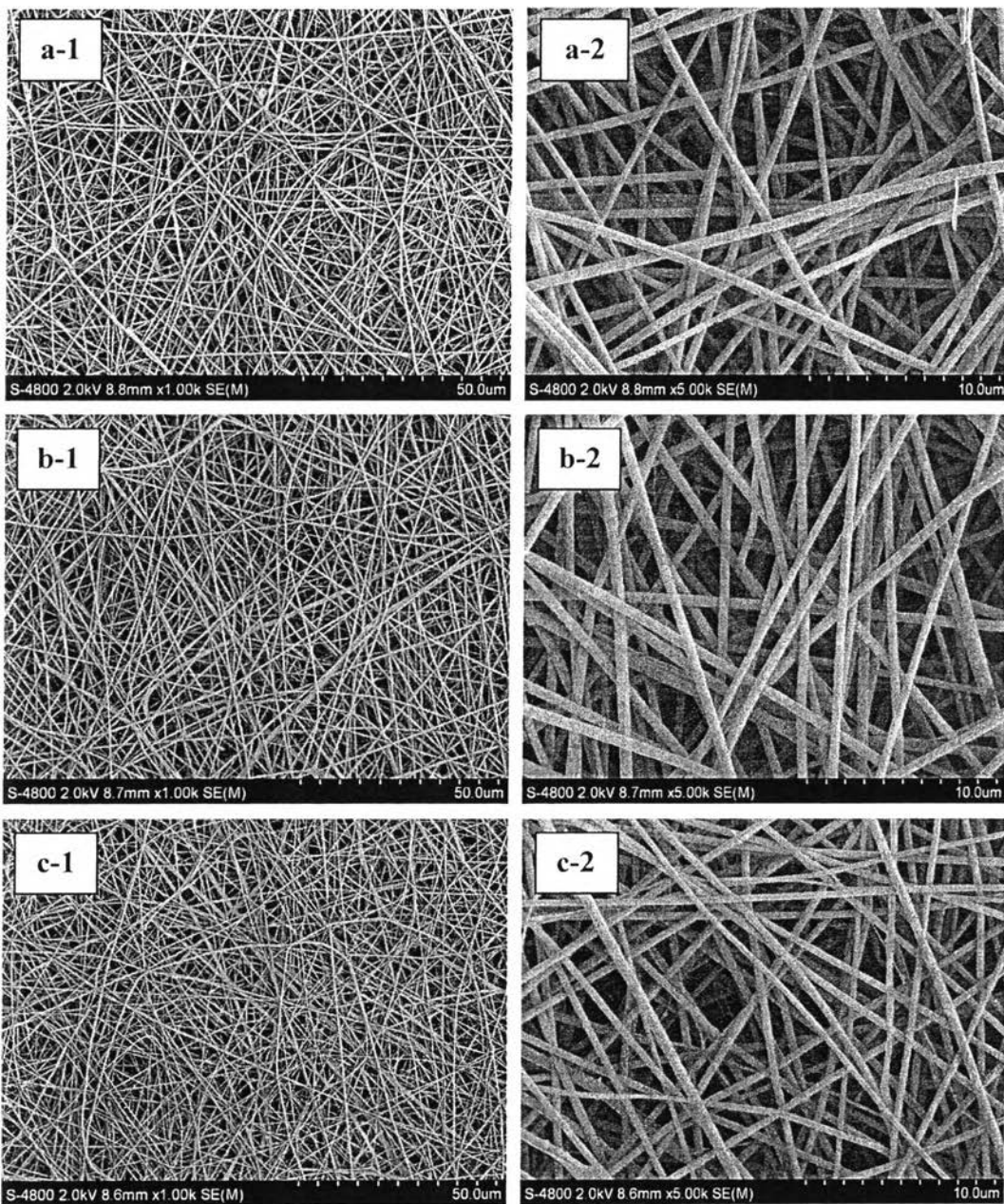
Temperature (°C) \ Time (h)	1	2	3
500	42.69	72.90	87.62
600	78.46	73.72	64.45
650	68.71	65.81	60.91

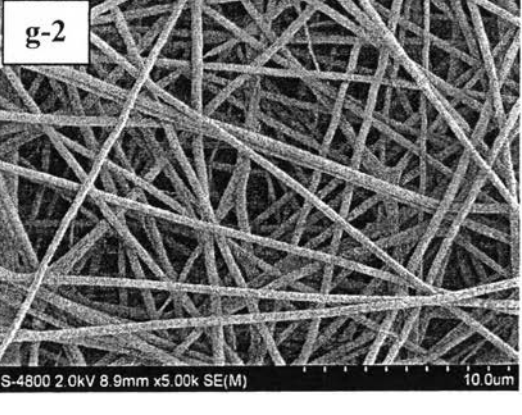
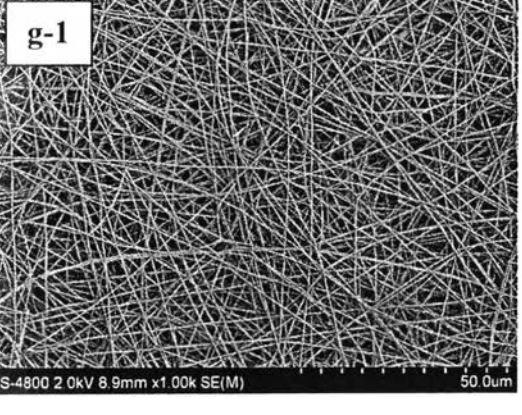
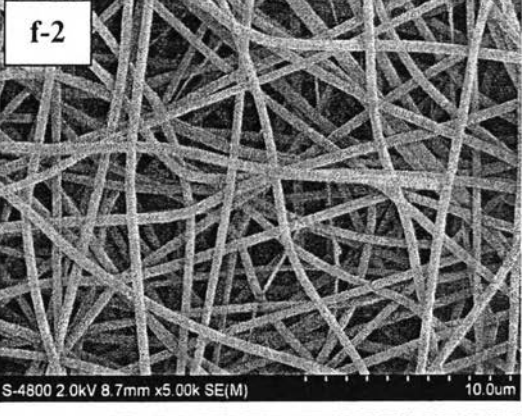
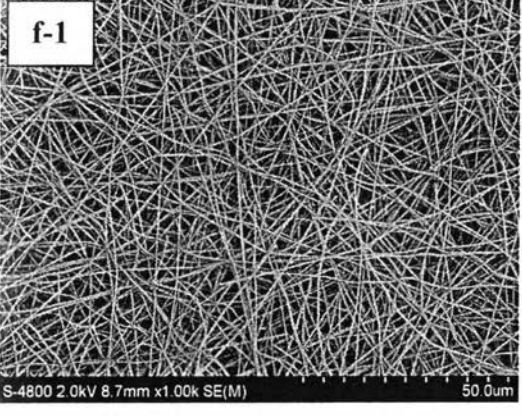
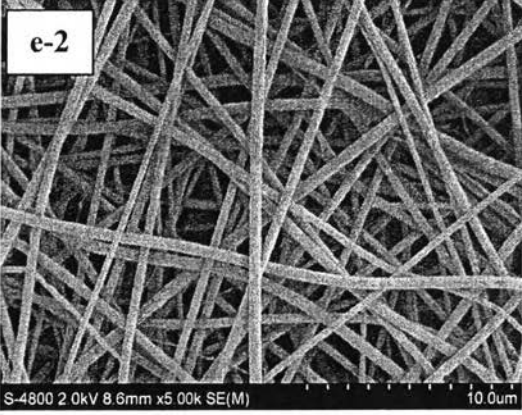
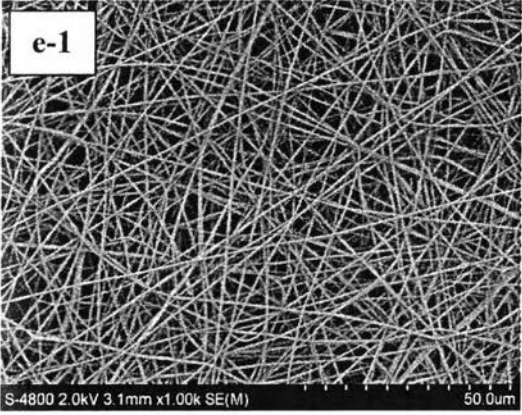
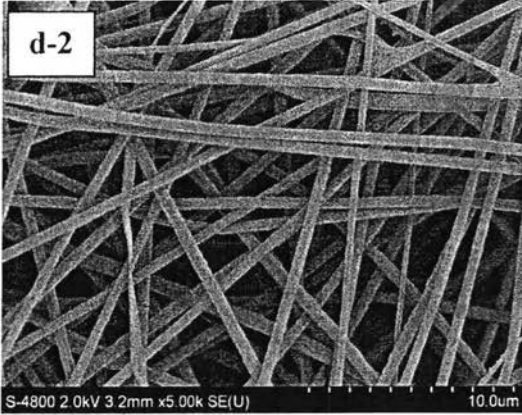
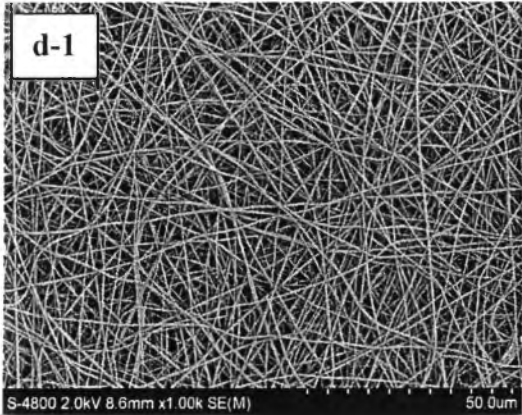
Table 4.3 The details of crystallite size at different conditions

Calcination condition	Crystallite size (nm)
500 °C 1 h	214.61
500 °C 2 h	259.59
500 °C 3 h	276.54
600 °C 1 h	208.59
600 °C 2 h	257.10
600 °C 3 h	261.28
650 °C 1 h	233.26
650 °C 2 h	285.37
650 °C 3 h	310.71

Figure 4.7 shows SEM images of the calcined TiO₂ hollow fibers (15 kV/17 cm) at different calcination conditions. From the results, the average diameters were going to be decreased after the calcination process due to the removal of organic content, which were PVAc matrix and mineral oil, from PVAc/Ti(ISO) composite fibers. Additionally, the higher the calcination time and temperature, the lower the average diameter got. Furthermore, the shrinkage occurred during the process as seen at the higher time and temperature of calcination conditions. As the time and temperature increased, the calcined fibers tended to be more rough and distorted. But the cracks were found at the calcination temperature up to 650 °C

for 3 h. The calcination process, however, does not significantly affect the structural nature of fibers. The relationships of the average diameter with respect to the calcination time and temperature are showed in Figure 4.8 and 4.9, respectively. The average diameters of fibers had a tendency to decline with increasing both calcination time and calcination temperature. Nonetheless, they slightly decreased in case of calcination time effect. The average diameter regarding the calcination time and temperature are also given in Table 4.4.





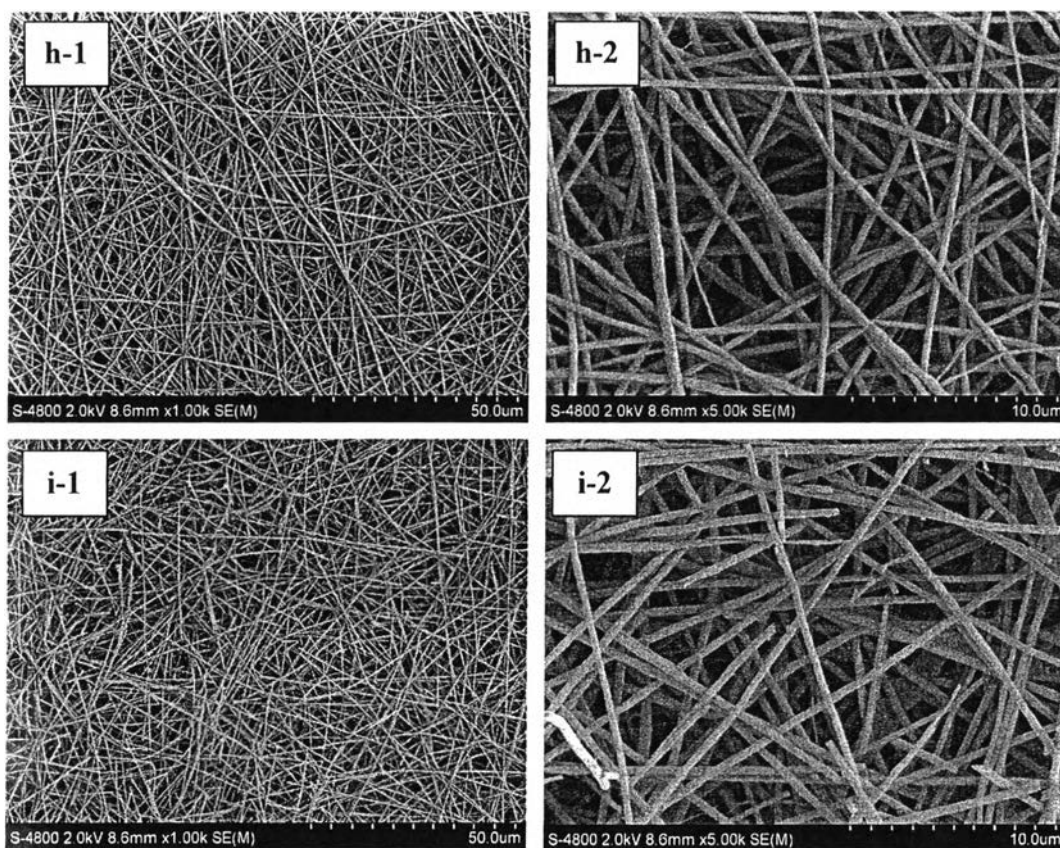


Figure 4.7 SEM images of the calcined TiO_2 hollow fibers (15 kV/17 cm) at different calcination conditions; at (a-1) low and (a-2) high magnifications of 500 °C/1h, at (b-1) low and (b-2) high magnifications of 500 °C/2h, at (c-1) low and (c-2) high magnifications of 500 °C/3h, at (d-1) low and (d-2) high magnifications of 600 °C/1h, at (e-1) low and (e-2) high magnifications of 600 °C/2h, at (f-1) low and (f-2) high magnifications of 600 °C/3h, at (g-1) low and (g-2) high magnifications of 650 °C/1h, at (h-1) low and (h-2) high magnifications of 650 °C/2h, and at (i-1) low and (i-2) high magnifications of 600 °C/3h.

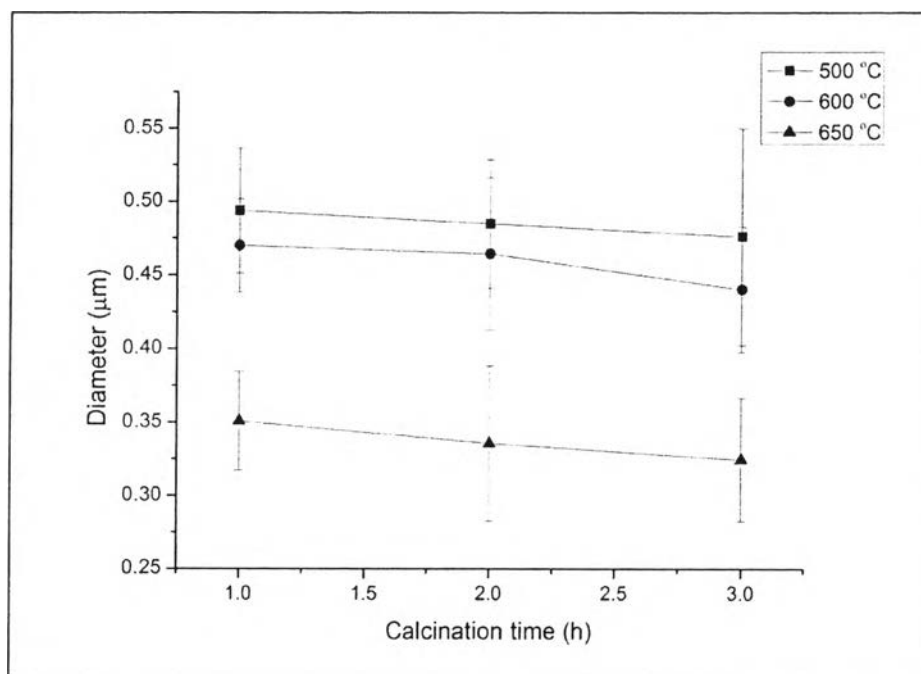


Figure 4.8 The average diameter of calcined TiO₂ hollow fiber at 500 °C, 600 °C, and 650 °C as a function of calcination time.

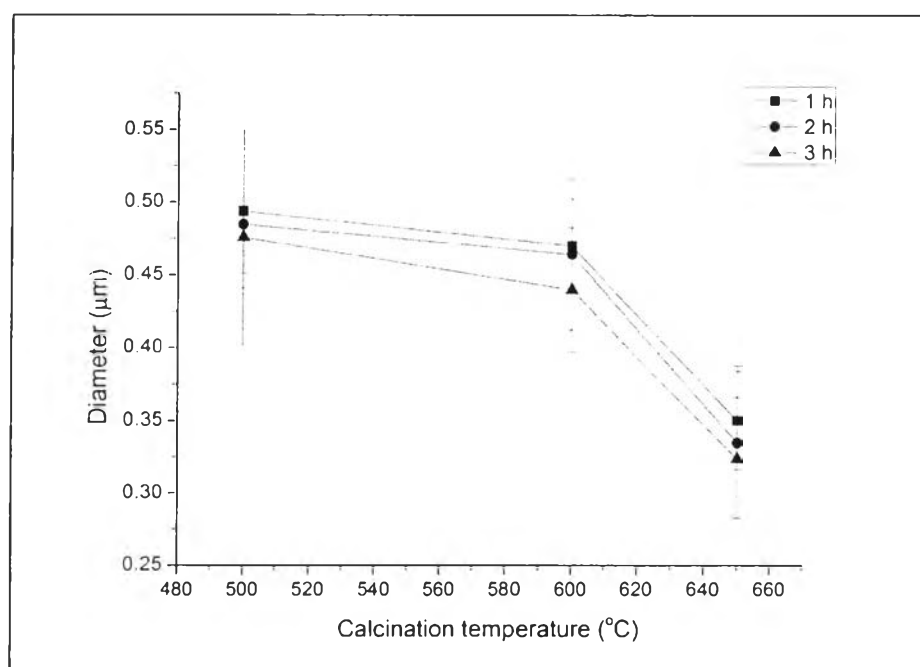


Figure 4.9 The average diameter of calcined TiO₂ hollow fiber at 1 h, 2 h, and 3 h as a function of calcination temperature.

Table 4.4 The average diameter (μm) of calcined TiO_2 hollow fibers at different calcination conditions

Temperature ($^{\circ}\text{C}$)	Time (h)		
	1	2	3
500	0.49 ± 0.04	0.48 ± 0.04	0.47 ± 0.07
600	0.47 ± 0.03	0.46 ± 0.05	0.44 ± 0.04
650	0.35 ± 0.03	0.33 ± 0.05	0.32 ± 0.04

Moreover, The IR spectroscopic analysis (see Figure 4.10) supported the successful removal of organic content after calcination process. The FT-IR spectrum with respect to the bending and stretching vibration of PVAc showed the absorption bands in the range of $1000\text{-}1750\text{ cm}^{-1}$ that evidently reduced after calcination process. On the contrary, the O-Ti-O bonding of anatase phase could be observed in the spectrum of around 470 cm^{-1} . Additionally, the FT-IR spectra of TiO_2 , Zn/TiO_2 and Ag/TiO_2 composite hollow fibers, which were obtained before and after the calcination, also exhibited the same results which shown in Figure 4.11, 4.12 and 4.13, respectively. The assignments for FT-IR absorption bands for poly(vinyl acetate) are showed in Table 4.5.

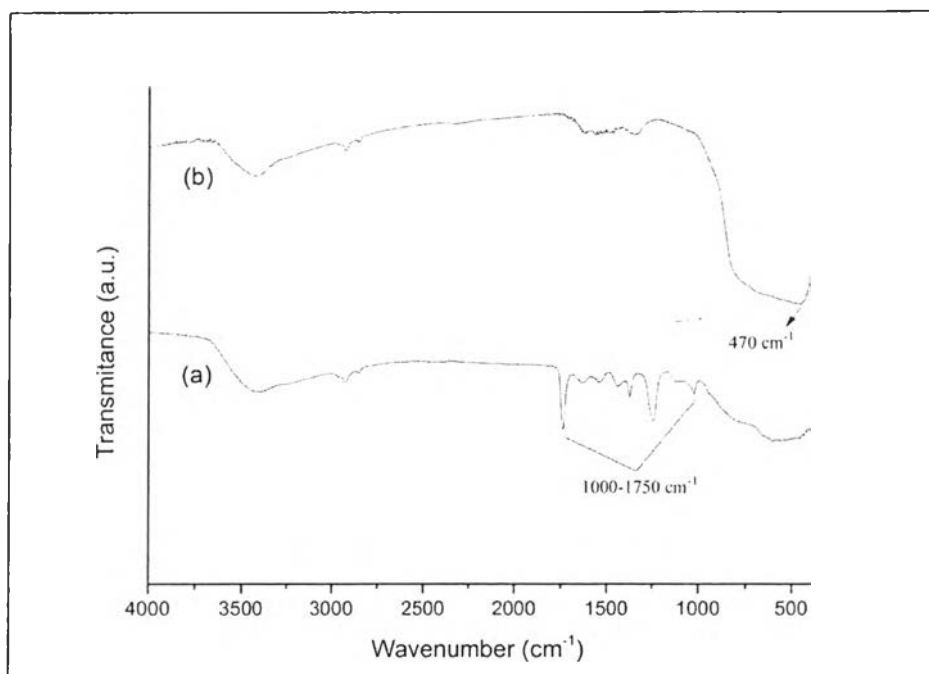


Figure 4.10 FTIR spectrum of (a) pre-calcined TiO₂ hollow fiber and (b) TiO₂ hollow fiber calcined at 500 °C 1 h. (The electrospinning condition was 15kV/17cm).

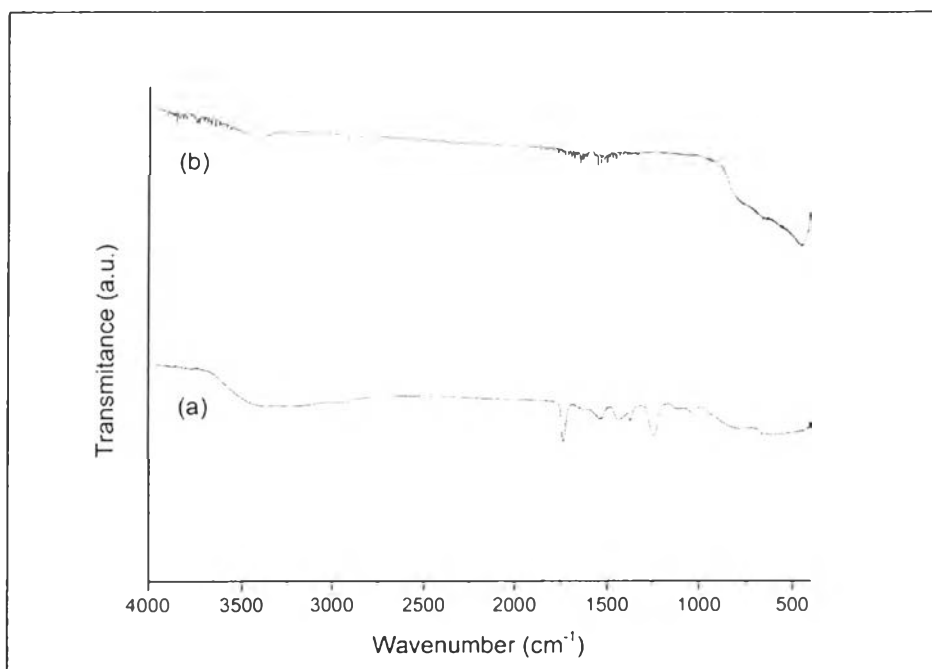


Figure 4.11 FTIR spectrum of (a) pre-calcined TiO₂ fiber and (b) TiO₂ fiber calcined at 500 °C 1 h. (The electrospinning condition was 15kV/17cm).

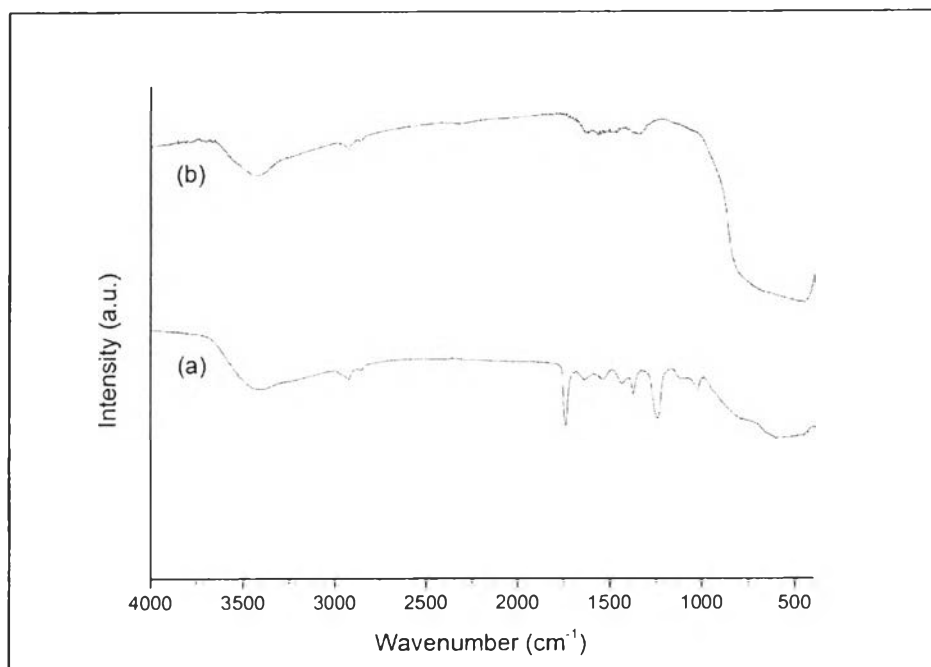


Figure 4.12 FTIR spectrum of (a) pre-calcined Zn/TiO₂ composite hollow fibers and (b) Zn/TiO₂ composite hollow fibers calcined at 500 °C 1 h. (The electrospinning condition was 15kV/17cm).

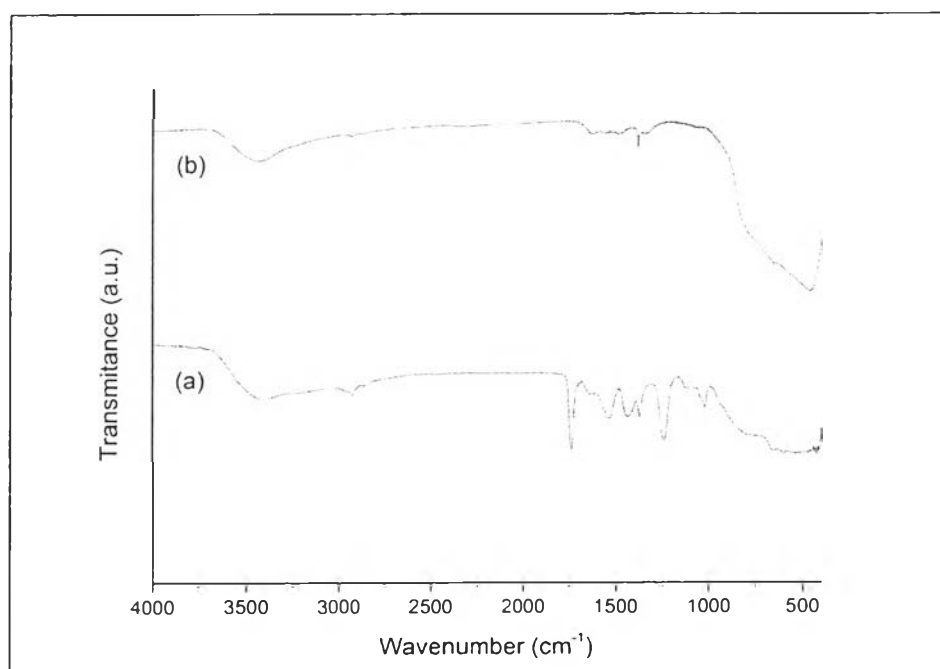


Figure 4.13 FTIR spectrum of (a) pre-calcined Ag/TiO₂ composite hollow fibers and (b) Ag/TiO₂ composite hollow fibers calcined at 500 °C 1 h. (The electrospinning condition was 15kV/17cm).

Table 4.5 Assignments for FT-IR absorption bands for poly(vinyl acetate) (Hatice and Olgun, 2011)

Wavelength (cm ⁻¹)	Assignment
2966-3700	CH ₃ and CH ₂ symmetric stretching
1742	C=O stretching
1435	CH ₃ stretching
1372	CH ₂ stretching
1232	C–O–C stretching
1018-944	CH ₂ asymmetric stretching

TiO₂ hollow fibers, Zn/TiO₂ composite hollow fibers, Ag/ TiO₂ composite hollow fibers as well as TiO₂ fibers were calcined in air atmosphere with a heating rate of 5 °C minute⁻¹ at 500 °C for 1 h which was the suitable calcination condition. It gave anatase phase and lowest crystallinity which were favorable for lithium ion insertion/deinsertion. Figure 4.14 presents the SEM images of TiO₂ hollow fibers, Zn/TiO₂ composite hollow fibers, Ag/ TiO₂ composite hollow fibers, and TiO₂ fibers that attained after the calcination. TiO₂ hollow fibers, TiO₂ fibers, and Zn/TiO₂ composite hollow fibers turned to the color of white while Ag/ TiO₂ composite hollow fibers had the color of gray. The average diameters of calcined fibers compared to that of pre-calcined ones were shown in Table 4.6. The results also confirmed the removal of organic content after the calcination leading to the reduction of fibers diameter.

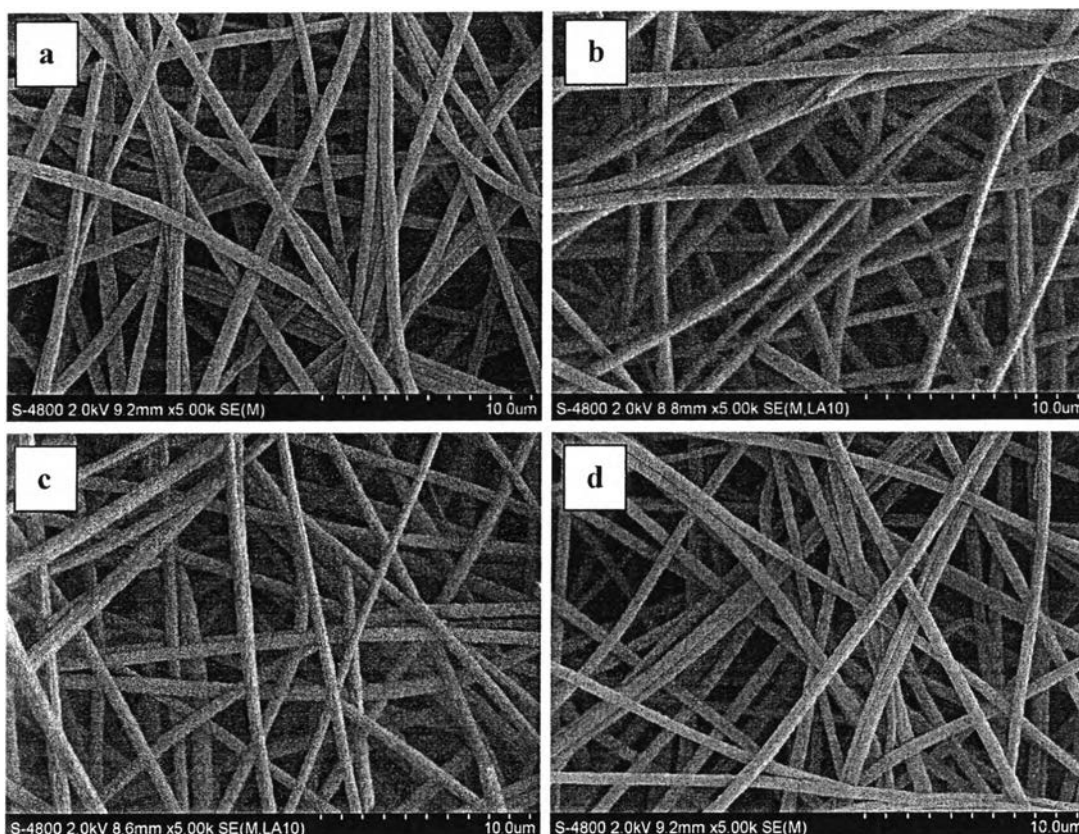


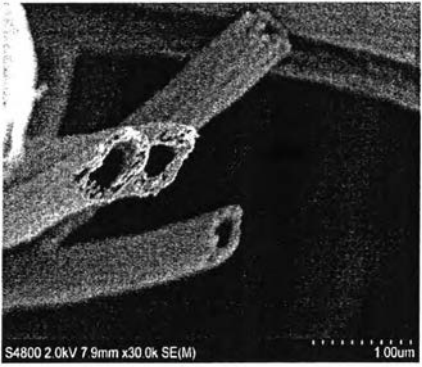
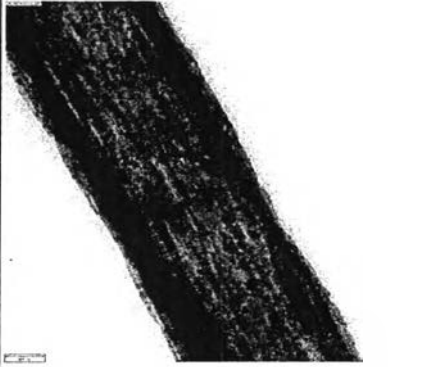
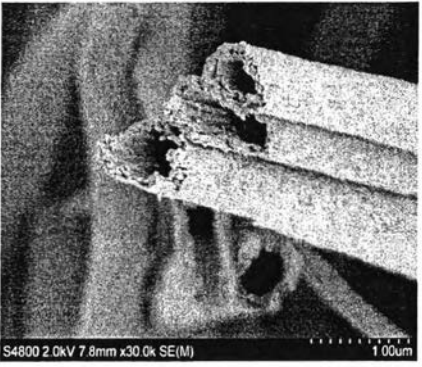
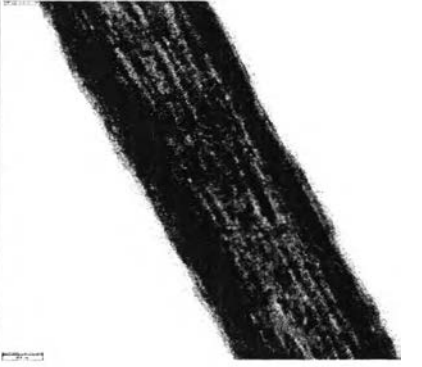

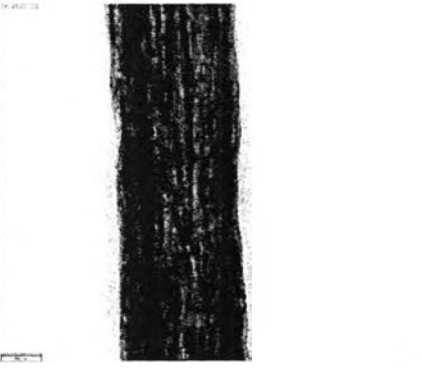
Figure 4.14 SEM images (magnification = 5000X; scale bar = 10.0 μm) of (a) calcined TiO_2 hollow fibers, (b) calcined Zn/ TiO_2 composite hollow fibers, (c) calcined Ag/ TiO_2 composite hollow fibers and (d) calcined TiO_2 fibers under the proper calcination condition of 500 $^\circ\text{C}$ for 1 h.

Table 4.6 The average diameter of fibers before and after calcination

Materials	The average diameter (μm)	
	Before calcination	After calcination
TiO_2 hollow fibers	0.91 ± 0.07	0.64 ± 0.04
Zn/ TiO_2 composite hollow fibers	0.90 ± 0.08	0.63 ± 0.05
Ag/ TiO_2 composite hollow fibers	0.87 ± 0.10	0.64 ± 0.05
TiO_2 fibers	0.91 ± 0.06	0.63 ± 0.05

In order to confirm the hollow structures of the produced fibers, cross sectional SEM images were examined as well (see Table 4.7). The existence of hollow structure attributed to the elimination of core that obtained after the calcination process. The properties of substance which served as core should have immiscibility with shell, adequate viscosity, and ease of removal. The obtained hollow fibers were composed of outer diameter of around $0.6\ \mu\text{m}$ with a wall thickness of around $0.1\ \mu\text{m}$. Furthermore, TEM images of selected individual fibers of calcined TiO_2 hollow fibers, Zn/TiO_2 composite hollow fibers, and Ag/TiO_2 composite hollow fibers were presented in Table 4.7. The TEM images supported the results of outer diameter and a wall thickness from cross sectional SEM images. Besides, the selective area electron diffraction (SAED) patterns (see Figure 4.15) of the calcined hollow fibers was observed. The results shown in Figure 4.15 (a) revealed the polycrystalline nature of anatase TiO_2 and the good crystallinity of the fibers got after calcination. Meanwhile, Figure 4.15 (b and c) represent the SAED patterns of calcined Zn/TiO_2 and Ag/TiO_2 composite hollow fibers. They also provided the same results as the case of calcined TiO_2 . To prove that the added zinc and silver particles have been oxidized and not vanished after being calcined, the FE-SEM EDX analysis was used. As the demonstrated results in Figure 4.16, zinc and silver metal were able to be discovered in the composite hollow fibers. These were assumed that zinc and silver metal were successfully oxidized and TiO_2 fibers composed of Zn and Ag nanoparticles which were eventually employed as seeds to outgrow the crystal on surface of TiO_2 hollow fibers. The atomic percentage of both calcined composite hollow fibers are shown in Table 4.8.

Table 4.7 Cross sectional SEM images and TEM images of calcined TiO₂ hollow fibers, Zn/TiO₂ composite hollow fibers, and Ag/TiO₂ composite hollow fibers

Materials	Cross sectional SEM images (Magnification = 30000X; scale bar = 1.00 μ m)	TEM images (Magnification = 10000X; scale bar = 200 nm)
TiO ₂ hollow fibers		
Zn/TiO ₂ composite hollow fibers		
Ag/TiO ₂ composite hollow fibers		

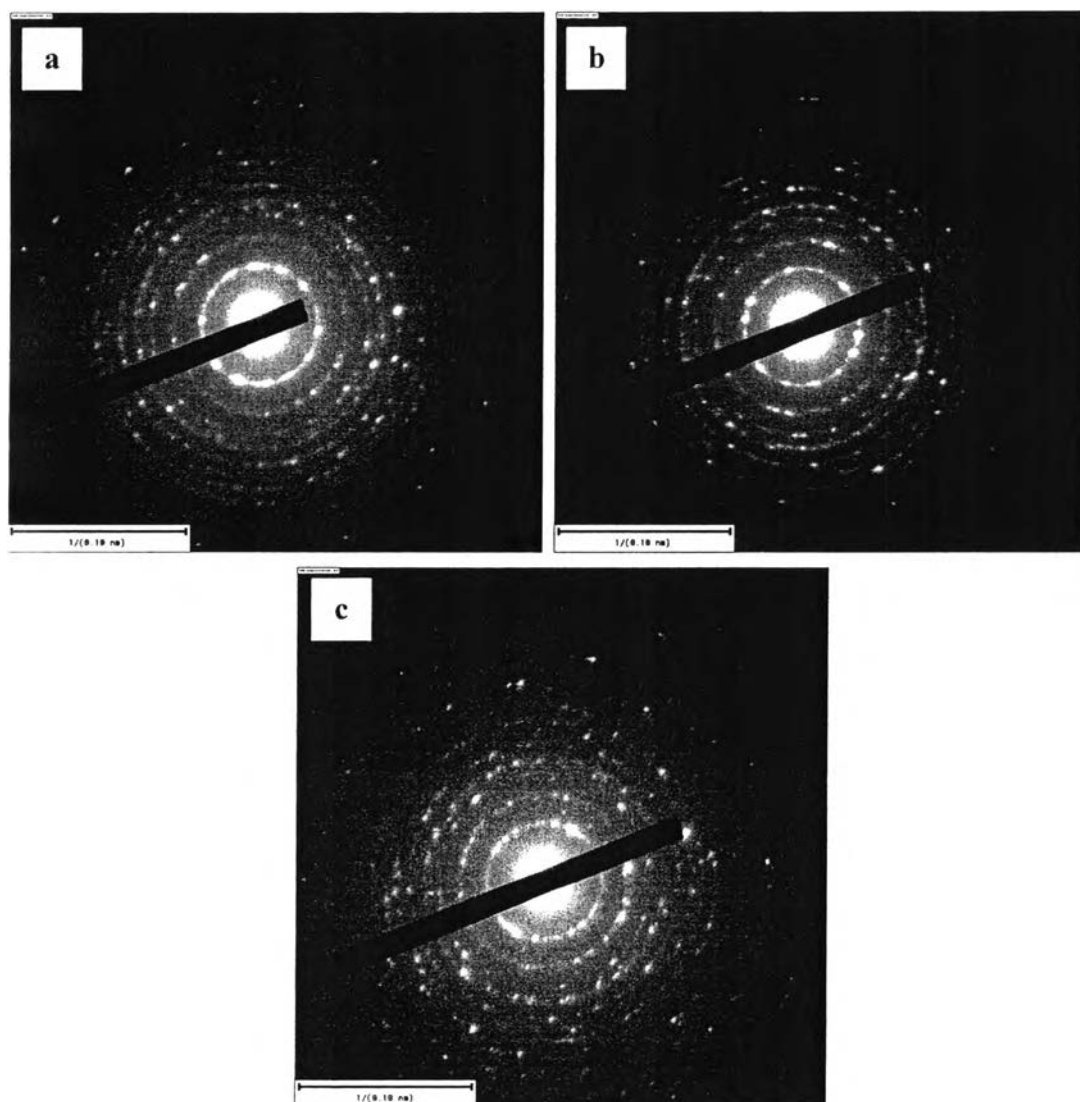
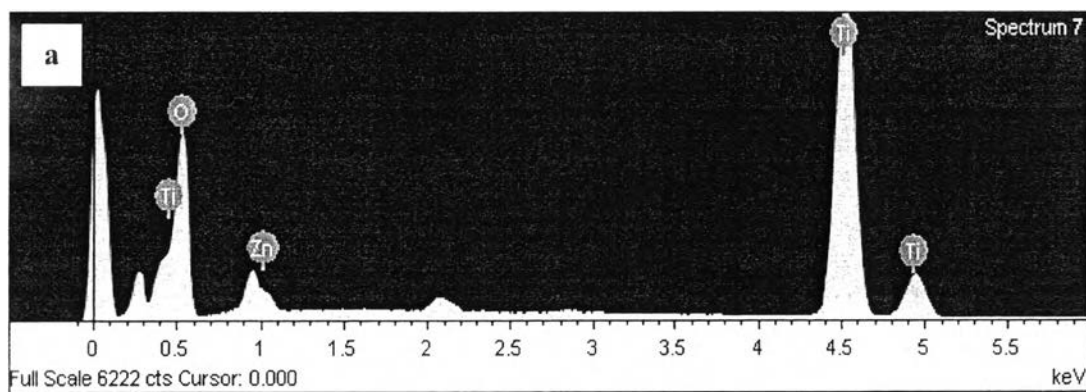


Figure 4.15 SAED patterns of (a) calcined TiO_2 hollow fibers, (b) Zn/TiO_2 composite hollow fibers, and (c) Ag/TiO_2 composite hollow fibers.



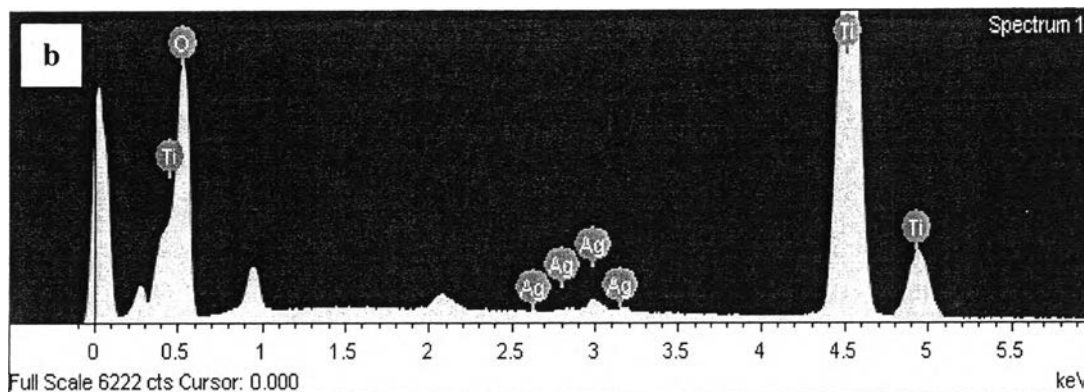


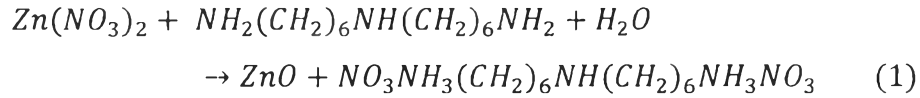
Figure 4.16 EDX results of (a) calcined Zn/TiO₂ composite hollow fibers and (b) Ag/TiO₂ composite hollow fibers.

Table 4.8 The atomic percentage of calcined composite hollow fibers

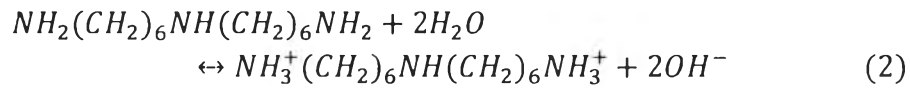
Atomic (%)	Materials					
	Zn/TiO ₂			Ag/TiO ₂		
	O	Ti	Zn	O	Ti	Ag
	51.37	48.45	0.18	51.82	47.73	0.45

4.3 The Effect of Surface Modification by Hydrothermal Treatment to the Morphology, Weight, and the Average Diameter of Synthesized ZnO/TiO₂ and Ag₂O/TiO₂ Composite Hollow Fibers

The hydrothermal treatment process has been aimed to be an effective means to synthesize fine ceramic materials. Generally, this process is operated in a close system at autogenous pressure. In this work, the calcined Zn-TiO₂ composite hollow fibers were treated with two chemicals; bis(hexamethylene)triamine (BHT) and zinc nitrate hexahydrate (ZNH) to produce zinc oxide outgrowths on surface of titanium oxide hollow fibers. Formation of ZnO from the combination of ZNH and BHT in aqueous medium can be illustrated by Eq. 1:



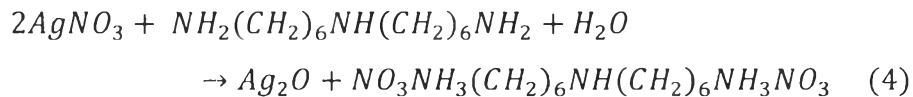
BHT, according to Eq. 1, acts as a base in the Brønsted-Lowry theory which is defined as a species with ability to accept proton. Eq. 2 shows hydrolyzing in water of BHT.



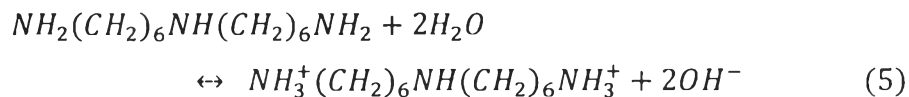
Then, zinc ions (Zn^{2+}) react with the hydroxide ions (OH^-) and form hydroxyl complexes $[\text{Zn}(\text{OH})_2]$ which ultimately transform into solid-phase according to Eq. 3.



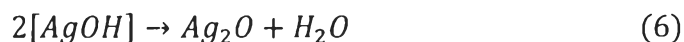
In consequence, the formation of ZnO, according to the above proposed mechanisms, is owing to the basicity of the reaction medium, which causes an increase in the concentration of the precursors (zinc hydroxyl complexes) and a rise in the chemical potential of hydroxide ions. In case of the growth mechanism of Ag_2O , the calcined Ag-TiO₂ composite hollow fibers were treated with BHT as same as Zn-TiO₂ composite hollow fibers but silver nitrate (AgNO_3) was use instead of ZNH. AgNO_3 provides Ag^+ ions required for building up silver oxide outgrowths on surface of titanium oxide hollow fibers. Formation of Ag_2O from the combination of AgNO_3 and BHT in aqueous solution can be described in Eq. 4:



And Eq. 5 shows hydrolyzing in water of BHT.



The hydroxide ions (OH^-) will react with silver ions (Ag^+) in the system to form hydroxyl complexes $[\text{AgOH}]$. The transformation into solid-phase of Ag_2O will be eventually occurred as shown in Eq. 6.



Therefore, the formation of Ag_2O crystal is capable of completing as the above mechanisms. Generally, the crystal growth contains two processes; nucleation and growth. The process of nucleation and growth normally take place in two different stages. In the first nucleation stage, a tiny nucleus, such as a dust particle, a small seed crystal, containing the newly forming crystal is created. Nucleation occurs relatively slowly as the initial crystal components. They impinge upon each other correctly in the direction of orientation and placement for them to adhere and form the crystal. After that, the second stage of growth rapidly follows. Crystal growth spreads outwards from the created nucleating sites.

4.3.1 Adjusting the Hydrothermal Treatment Condition under the Fixed Time for 1 Hour at Various Temperatures

4.3.1.1 ZnO Outgrowths

The calcined Zn/TiO₂ composite hollow fibers were allowed to undergo hydrothermal treatment for 1 h at different temperatures. Zn metals were purposely added as seeds to provide nucleation sites for facilitating crystal growth. SEM images of the hydrothermally treated products were exhibited in Figure 4.17. According to the SEM results, flower-like outgrowths were grown all over the TiO₂ surface and there is noteworthy that ZnO-TiO₂ composite hollow fibers have been treated by hydrothermal technique, the hollow structure still be remained though. In addition, The average fibers diameter (see Figure 4.18) became bigger as a function of temperature due to the growth of ZnO grains. However, there was substantially varied in size at the reaction temperature from 110 °C to 115 °C. ZnO grains growth were increased in size of grains at higher temperature, accompanied by a reduction in the number of grains per volume, then the total area of grain boundary would be decreased.

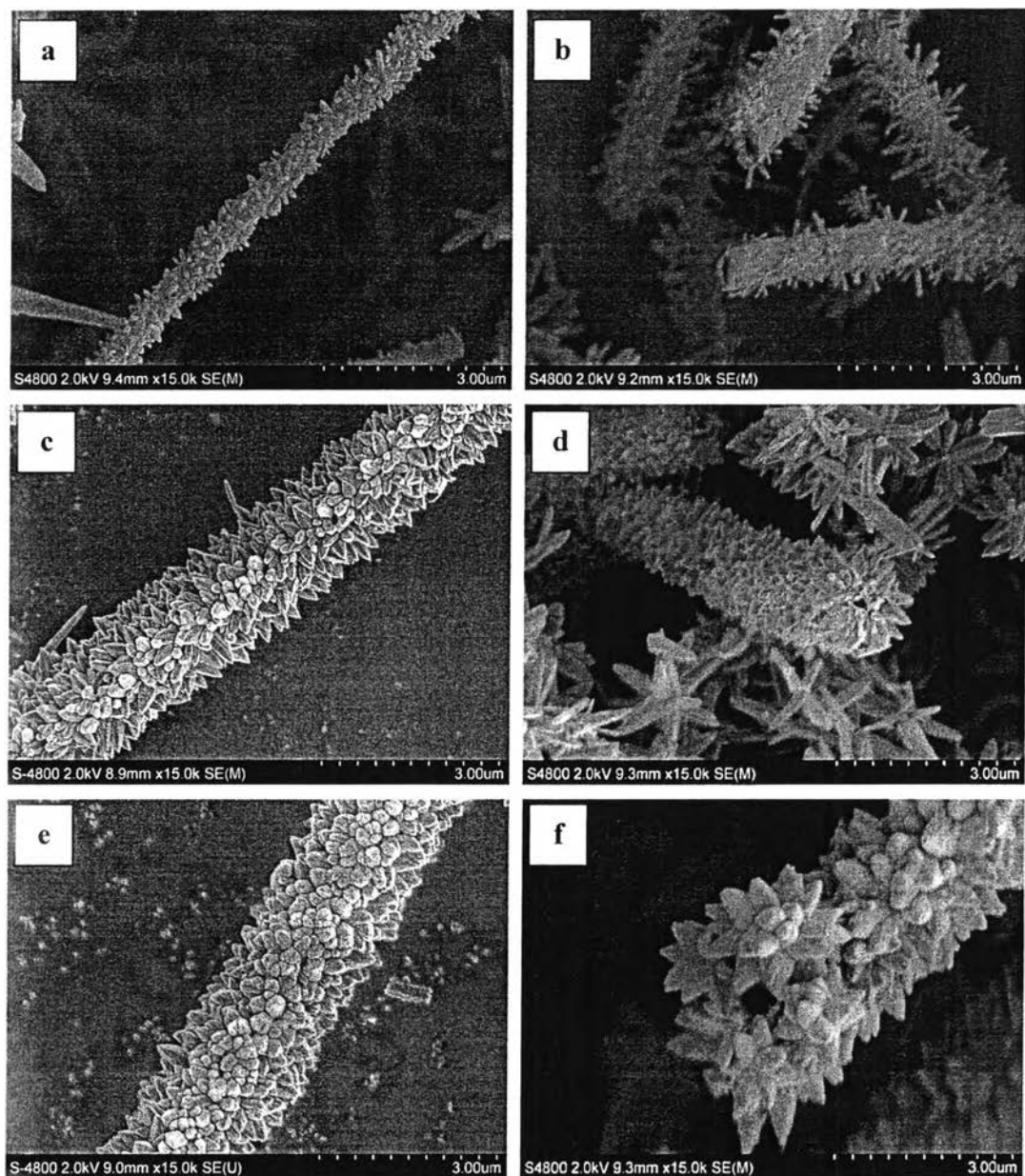


Figure 4.17 SEM images (magnification = 15000X; scale bar = 3.00 μm) of hydrothermally treated ZnO-TiO₂ composite hollow fibers for 1 h at (a and b) 110 °C, (c and d) 115 °C, and (e and f) 120 °C.

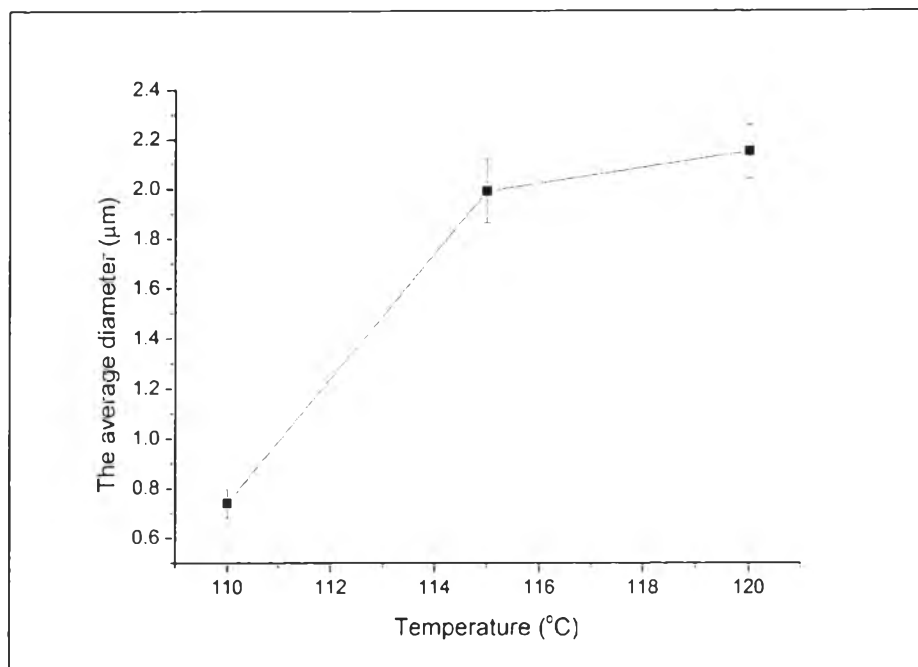


Figure 4.18 The average diameter of hydrothermally treated ZnO-TiO₂ composite hollow fibers for 1 h at various temperatures.

Table 4.9 The average diameter of ZnO-TiO₂ composite hollow fibers after hydrothermal treatment for 1 h

Temperature (°C)	The average diameter (μm)
110	0.74 ± 0.06
115	1.99 ± 0.13
120	2.15 ± 0.11

After undergoing of hydrothermal treatment, the obtained weight of ZnO outgrowths became higher. It could be indicated that the higher temperature led to a rise in weight because of the growth of crystals. But it had a notice at the temperature of 120 °C, weight became lower. This result probably occurred from the slightly decomposition of zinc nitrate precursor at high temperature reaching to 120 °C. The relationship between temperature and weight is illustrated in Figure 4.19.

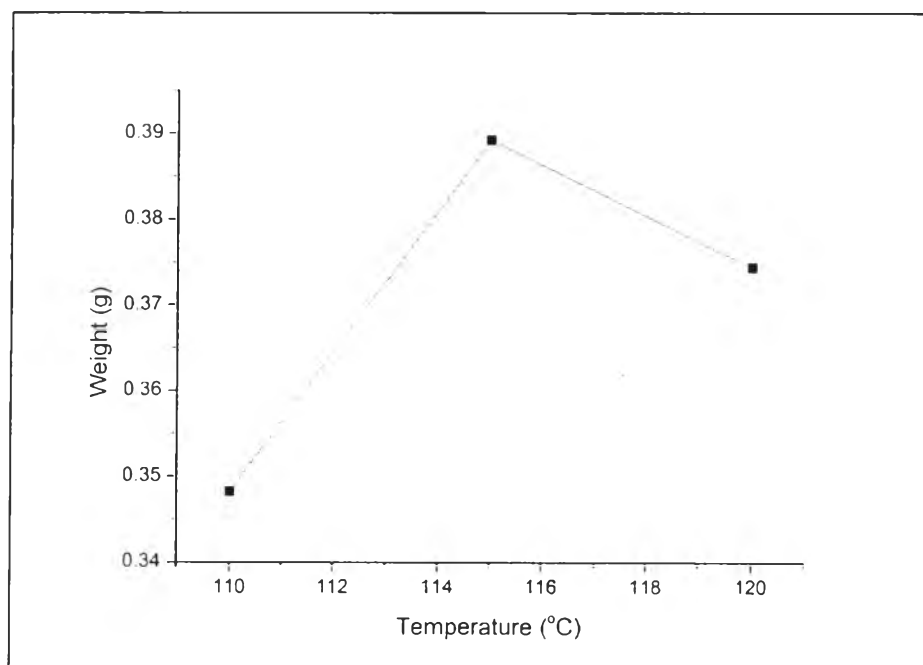


Figure 4.19 The obtained weight of ZnO outgrowths for 1 h at different temperatures.

Table 4.10 The weight of ZnO-TiO₂ composite hollow fibers before and after hydrothermal treatment for 1 h

Temperature (°C)	Weight (g)		
	before	after (without precursor)	After (with precursor)
110	0.0100	0.0073	0.3555
115	0.0100	0.0060	0.3952
120	0.0100	0.0051	0.3795

So as to ensure that ZnO branching was comprised of pure zinc oxide, EDX analysis has been measured. Figure 4.20 (a-c) showed the high intensity of zinc signals at the outgrowing branches. Likewise, they represented the almost absent titanium peaks. In consequence, it suggested that ZnO branches created from hydrothermal treatment contained no titanium-content.

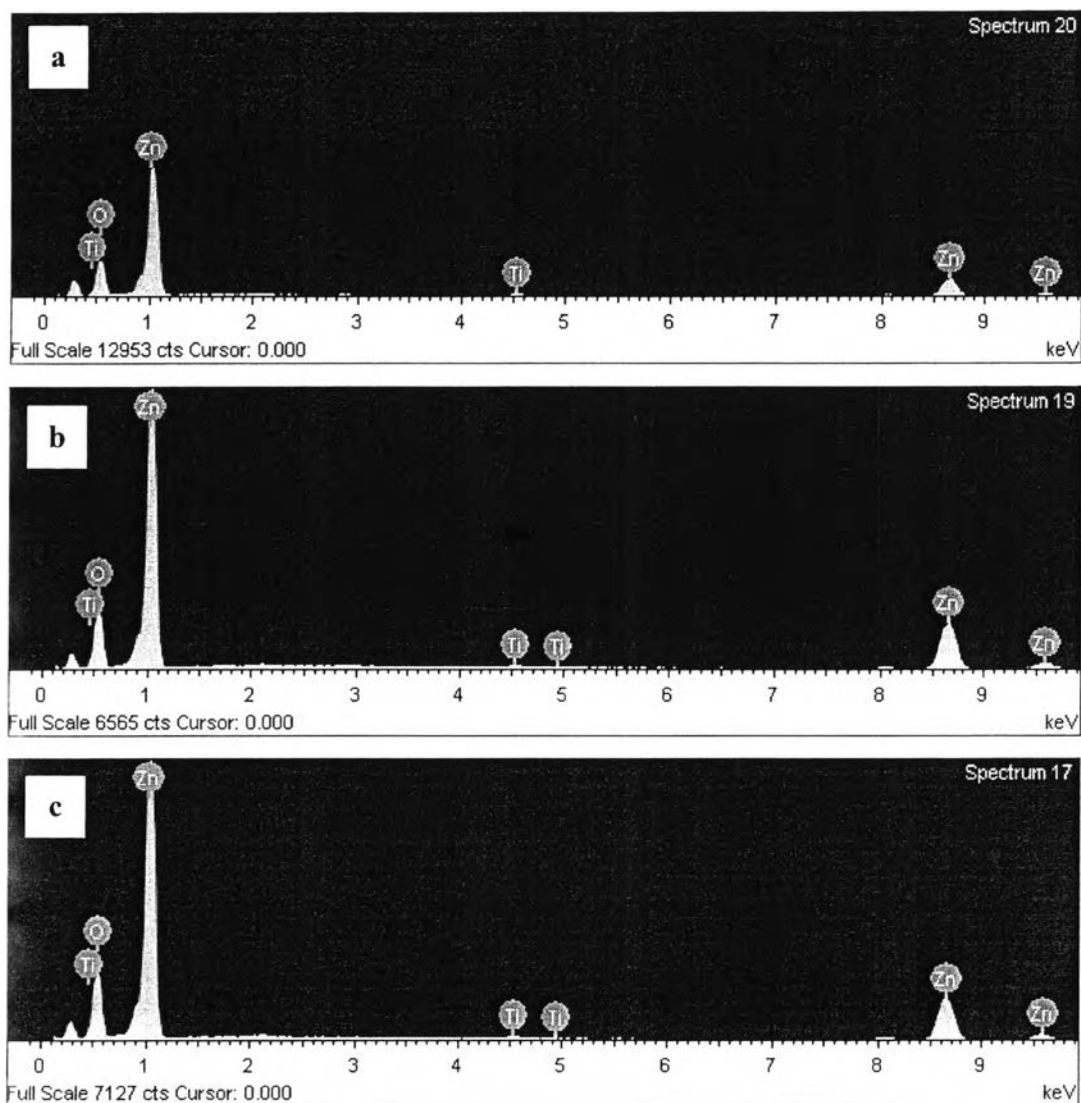


Figure 4.20 EDX results of hydrothermally treated ZnO-TiO₂ composite hollow fibers for 1 h at (a) 110 °C, (b) 115 °C, and (c) 120 °C.

Table 4.11 The atomic percentage of hydrothermally treated ZnO-TiO₂ composite hollow fibers for 1 h at various temperatures

Atomic (%)	Temperature (°C)								
	110			115			120		
	O	Ti	Zn	O	Ti	Zn	O	Ti	Zn
	55.00	3.48	41.52	48.46	2.75	48.79	52.12	2.54	45.33

Furthermore, XRD patterns of Zn/TiO₂ composite hollow fibers obtained after calcination and ZnO-TiO₂ composite hollow fibers obtained after hydrothermal treatment for 1 h at various temperatures are also observed in Figure 4.21. Pattern (a) represents XRD pattern of the calcined Zn/TiO₂ composite hollow fibers which the anatase phase of titanium oxide has been attained. The appearance of crystalline peaks at 2θ degree of 25.35°, 37.951°, 48.092°, 54.089°, 55.135°, 70.314°, and 75.153° which referred to the crystal planes of (101), (004), (200), (105), (211), (220), and (215) revealed the formation of anatase phase without contamination of other phases (JCPDS card No 21-1272). Nonetheless, there was peak corresponding to ZnO appeared in pattern (a) which carried a small intensity. This appearance of ZnO peak can be indicated that the calcined fibers contain zinc oxide in the form of dispersed nanoparticles. This finding could support the EDX results as above-mentioned. Additionally, from the pattern (b-d), the newly created peaks after the hydrothermal treatment process at different temperatures supported the formation of zinc oxide as reported in JCPDS card No 36-1451. All diffraction peaks indicate that the created ZnO was monophasic zincite with a hexagonal structure. The peak with regard to anatase titanium oxide, however, could be found in these three patterns. The formation of ZnO nanobranches was further supported by TEM observation which can be normally used to discriminate between the crystalline and amorphous structures of materials. Figure 4.22 shows the SAED patterns of the hydrothermally treated ZnO-TiO₂ composite hollow fibers at 110 °C, 115 °C, and 120 °C. According to the results, the good crystallinity of synthesized fibers could be observed. Moreover, the crystallite size of ZnO outgrowths after hydrothermal treatment at various temperatures were calculated by the Scherrer's equation of the peaks regarding ZnO which correspond to the crystal plane of (101) and displayed in Table 4.12. The results revealed that crystallite size increased with increasing the reaction temperature. Nonetheless, at 120 °C, crystallite size started to declined probably due to the decomposition of precursor together with the damage of the crystals.

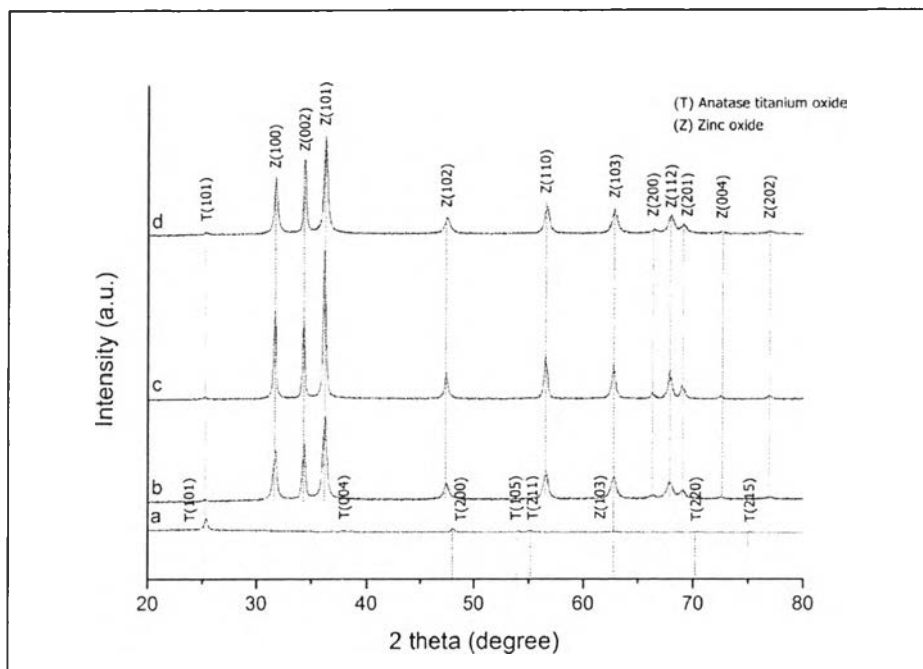
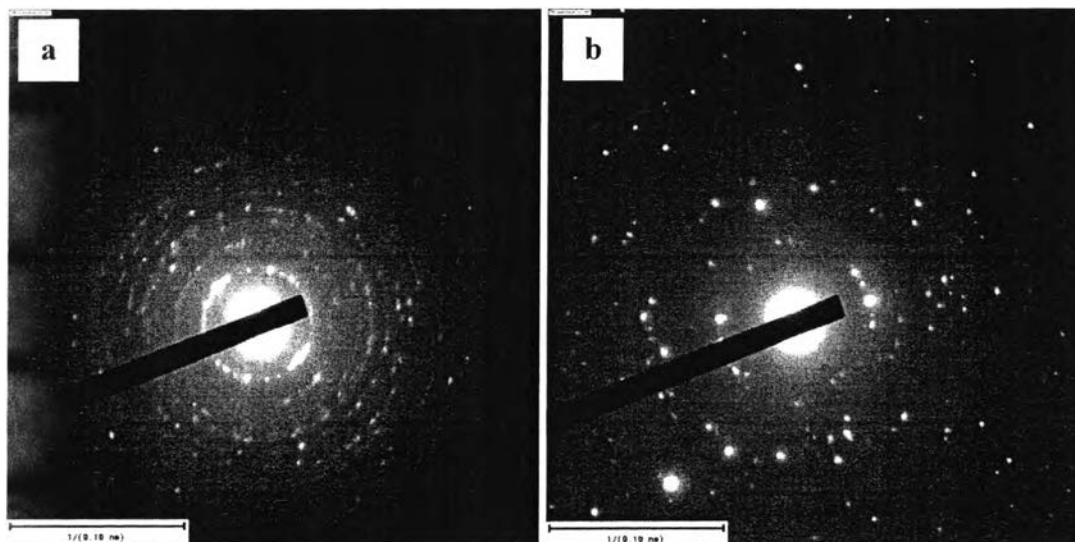


Figure 4.21 XRD patterns of (a) Zn/TiO₂ composite hollow fibers obtained after calcination and ZnO-TiO₂ composite hollow fibers obtained after hydrothermal treatment for 1 h at (b) 110 °C, (c) 115 °C, and (d) 120 °C.



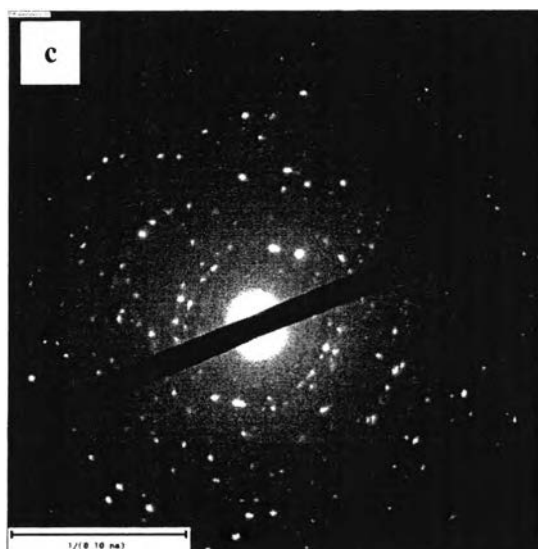


Figure 4.22 SAED patterns of ZnO-TiO₂ composite hollow fibers obtained after hydrothermal treatment for 1 h at (a) 110 °C, (b) 115 °C, and (c) 120 °C.

Table 4.12 The crystallite size of ZnO outgrowths at various temperatures

Temperature (°C)	Crystallite size (nm)
110	212.40
115	286.86
120	211.54

4.3.1.2 Ag₂O Outgrowths

The calcined Ag/TiO₂ composite hollow fibers were also allowed to treat by hydrothermal treatment for 1 h at different temperatures creating Ag₂O crystals on TiO₂ fiber surface. Ag metals were employed as seeds for crystal growth. The products attained after undergoing of hydrothermal treatment showed cubic-like outgrowths of Ag₂O spreading thoroughly on the surface of TiO₂ fibers with the remained hollow structures as can be clearly seen in Figure 4.23 of SEM images. Moreover, the average fibers diameter are investigated as well in Figure 4.24 which gives the relationship between temperature and the average diameter of the products.

In consequence of a rise in temperature, the average diameter of $\text{Ag}_2\text{O-TiO}_2$ composite hollow fibers increased. The reason for the increasing in diameter should be noted that temperature had ability to affect the growth of Ag_2O grains with respect to the reducing of grain boundary at the higher temperature. These results were similar to the case of ZnO outgrowths.

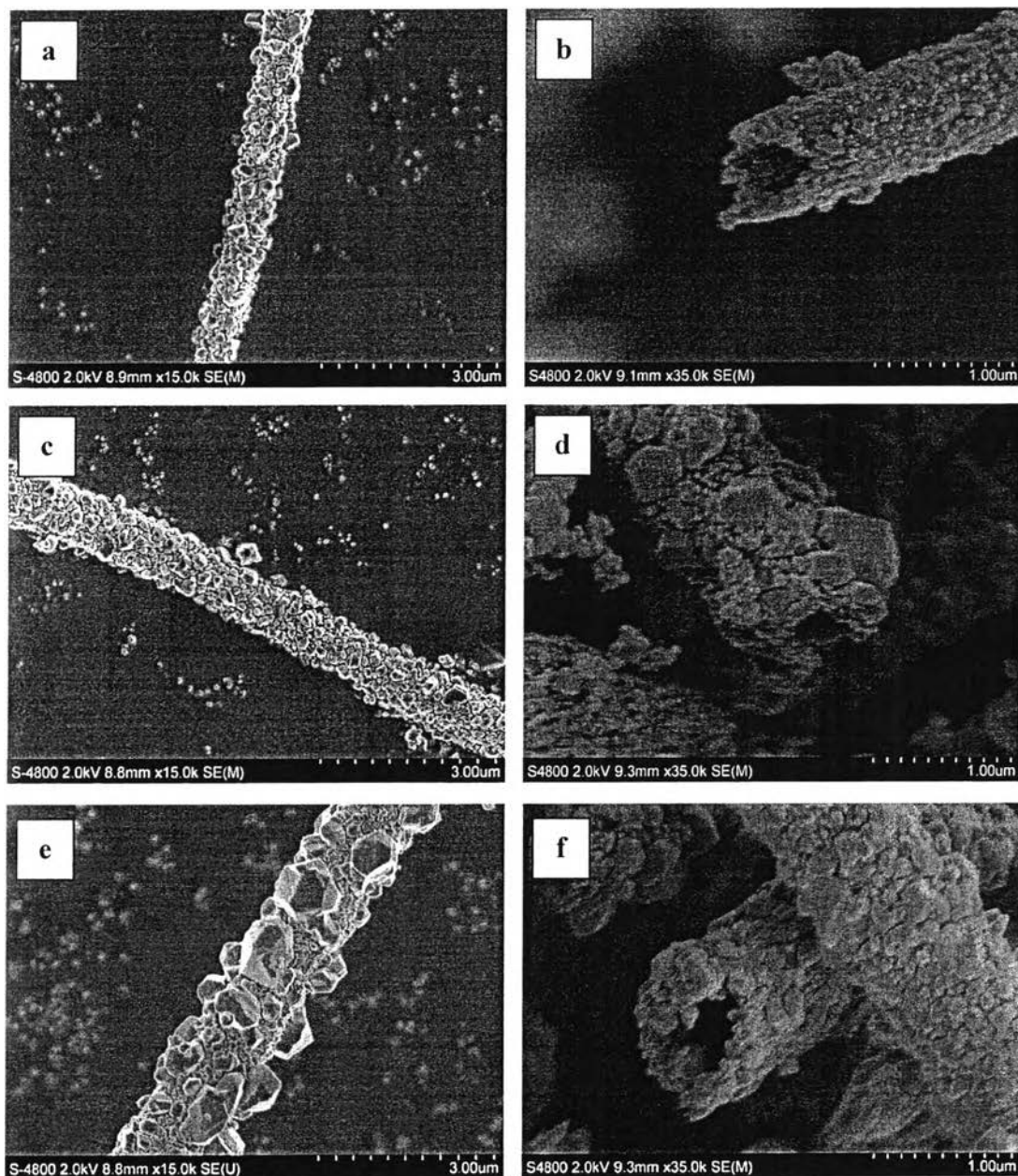


Figure 4.23 SEM images of hydrothermally treated $\text{Ag}_2\text{O-TiO}_2$ composite hollow fibers for 1 h at (a) 110 °C, (c) 115 °C, and (e) 120 °C at magnification = 15000X;

scale bar = 3.00 μm and at (b) 110 $^{\circ}\text{C}$, (d) 115 $^{\circ}\text{C}$, and (f) 120 $^{\circ}\text{C}$ at magnification = 35000X; scale bar = 1.00 μm .

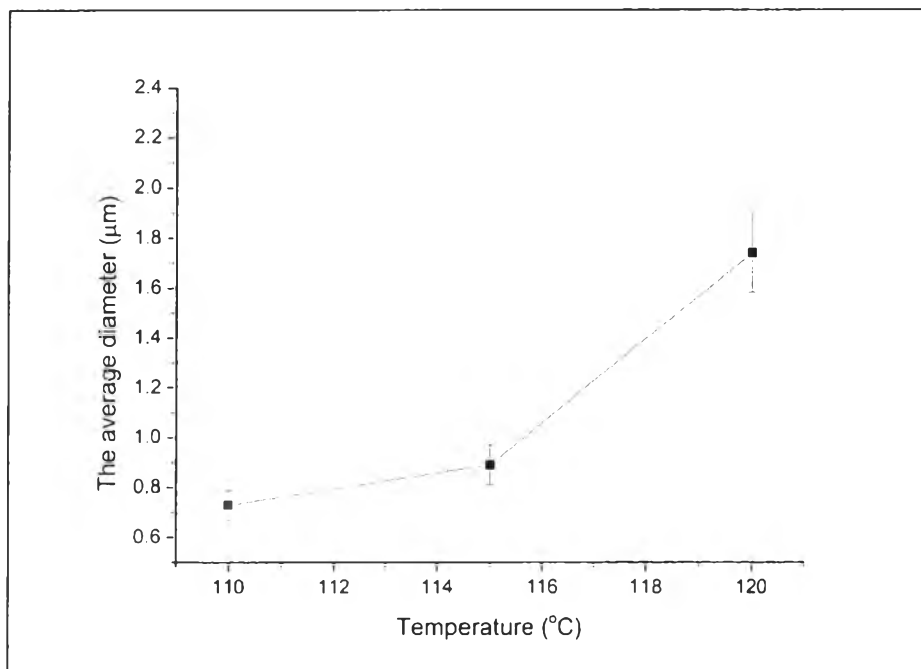


Figure 4.24 The average diameter of hydrothermally treated $\text{Ag}_2\text{O-TiO}_2$ composite hollow fibers for 1 h at various temperatures.

Table 4.13 The average diameter of $\text{Ag}_2\text{O-TiO}_2$ composite hollow fibers after hydrothermal treatment for 1 h

Temperature ($^{\circ}\text{C}$)	The average diameter (μm)
110	0.73 \pm 0.06
115	0.89 \pm 0.08
120	1.74 \pm 0.16

Figure 4.25 displays the relationship between temperature and weight of Ag_2O outgrowths obtained after hydrothermal treatment process. As the result, the weight became higher since the temperature went up. The weight of materials prior to the pre-hydrothermal treatment and hydrothermally treated ones

are showed in Table 4.14. It could be recommended that the higher the temperature of an operation, the more the weight of crystals they gained. It resulted from the growth of crystals getting larger and higher.

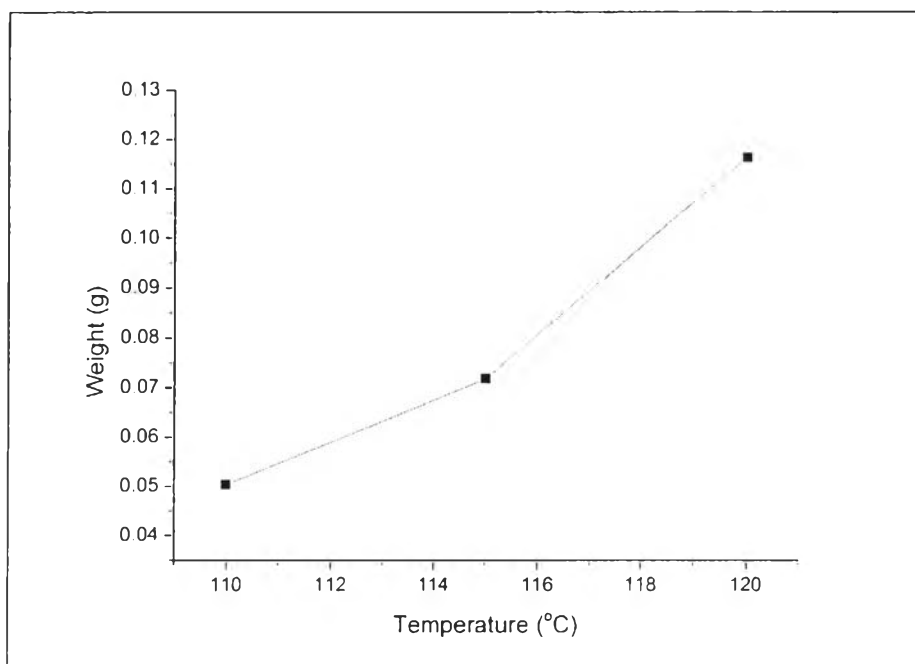


Figure 4.25 The obtained weight of Ag_2O outgrowths for 1 h at various temperatures.

Table 4.14 The weight of Ag_2O - TiO_2 composite hollow fibers before and after hydrothermal treatment for 1 h

Temperature (°C)	Weight (g)		
	before	after (without precursor)	After (with precursor)
110	0.0100	0.0069	0.0574
115	0.0100	0.0061	0.0780
120	0.0100	0.0048	0.1211

EDX analysis has been utilized in order to confirm that Ag_2O outgrowths contain silver oxide. The strong intensity of silver peaks at the outgrowing parts could be observed as obviously seen Figure 4.26 (a-c). They exhibited the higher intensity in comparison with the pre-hydrothermally treat ones. Other than that titanium and oxide peaks were also detected. Thus, hydrothermal treatment was found to be necessary for growing out the crystals.

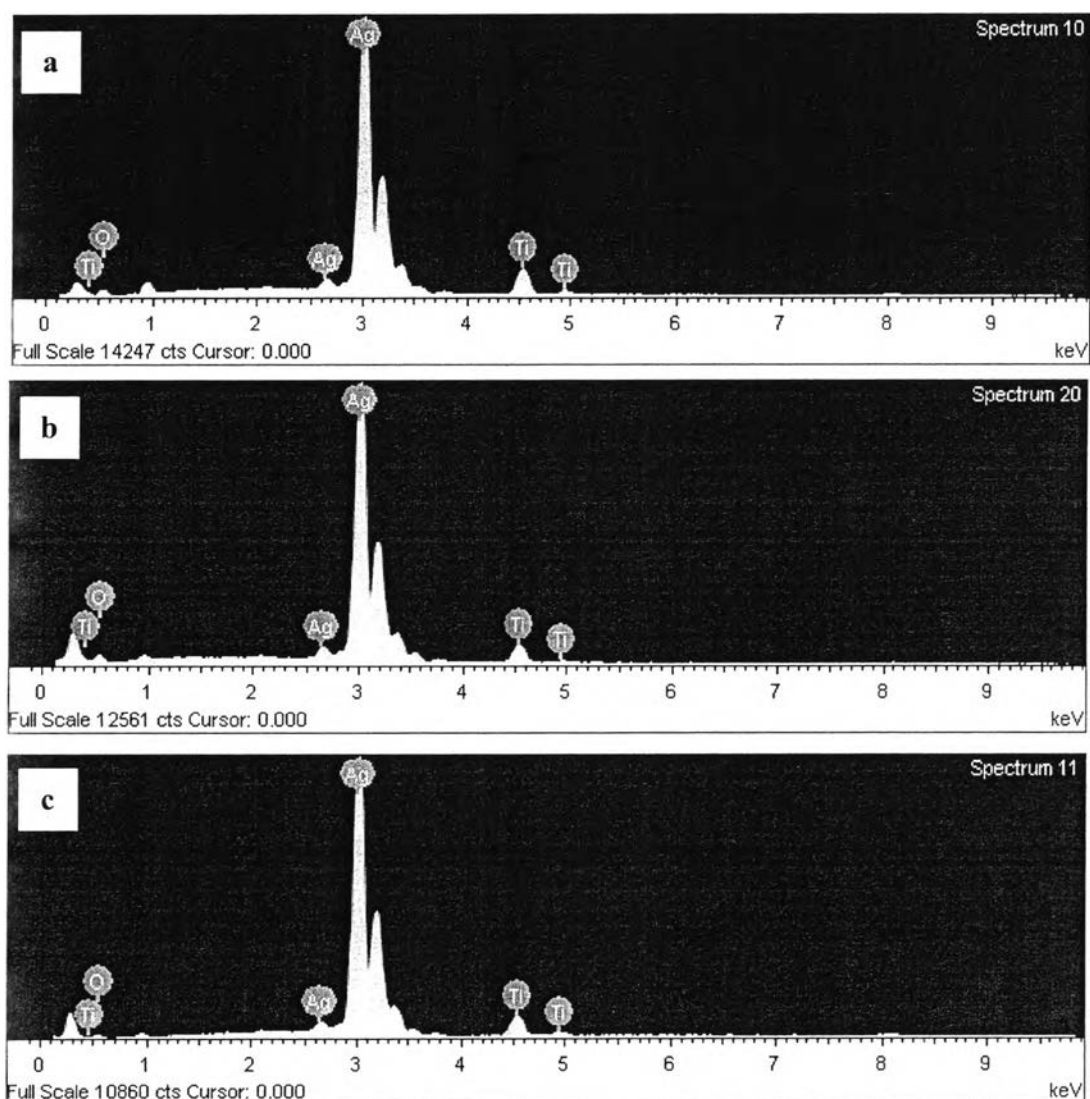


Figure 4.26 EDX results of hydrothermally treated Ag_2O - TiO_2 composite hollow fibers for 1 h at (a) 110 °C, (b) 115 °C, and (c) 120 °C.

Table 4.15 The atomic percentage of hydrothermally treated $\text{Ag}_2\text{O-TiO}_2$ composite hollow fibers for 1 h at different temperatures

Atomic (%)	Temperature (°C)								
	110			115			120		
	O	Ti	Ag	O	Ti	Ag	O	Ti	Ag
	10.38	17.77	71.96	11.54	12.96	75.50	7.88	12.49	79.62

Figure 4.27 manifests XRD patterns of Ag/TiO_2 composite hollow fibers which acquired after calcination and $\text{Ag}_2\text{O-TiO}_2$ composite hollow fibers obtained after hydrothermal treatment for 1 h at different temperatures. According to the pattern (a) that represents XRD pattern of the calcined Ag/TiO_2 composite hollow fibers, the crystalline peaks of the anatase phase of titanium oxide has been attained at 2θ degree of 25.211° , 37.771° , 38.427° , 47.947° , 53.874° , 54.993° , 62.105° , 62.666° , 68.752° , 70.191° , 75.208° and 76.039° corresponded to the crystal planes of (101), (004), (112), (200), (105), (211), (213), (204), (116), (220), (215), and (311). The visible peaks ensure that the formation of anatase phase consisted of no other phases (JCPDS card No 21-1272). The existence of Ag_2O peaks were also discovered in pattern (a) at 2θ degree of 37.991° , 44.14° , 64.372° , and 77.301° corresponding to the crystal planes of (111), (200), (220), and (311). The barely presence of this oxide could be implied that, after calcination, silver oxide in the form of dispersed nanoparticles appeared in the composite fibers which can also be confirmed by the EDX results as the mentioned before. In accordance with the XRD pattern (b-d), after the hydrothermal treatment process at different temperatures, the peaks of Ag_2O increased in intensity of 3C silver with a cubic crystal structure (JCPDS card No 04-0783). As the obtained results, undergoing of hydrothermal treatment caused a rise in intensity of peaks which compared to the pre-hydrothermally treated ones. Increasing in intensity denoted that the crystallinity became higher. Furthermore, some peaks with respect to anatase titanium oxide were retained. The SAED patterns of the hydrothermally treated $\text{Ag}_2\text{O-TiO}_2$ composite hollow fibers at 110°C , 115°C , and 120°C were further illustrated in Figure 4.28.

The results clearly suggested the confirmation that the synthesized composted hollow fibers comprised of good crystallinity. Furthermore, the crystallite size of Ag_2O outgrowths after hydrothermal treatment at various temperatures were calculated by the Scherrer's equation of the peaks regarding to Ag_2O which correspond to the crystal plane of (111) and showed in Table 4.16. The results suggested that crystallite size increased as the reaction temperature increased. These could confirm the increasing in the average diameter and the obtained weight of crystals outgrowths.

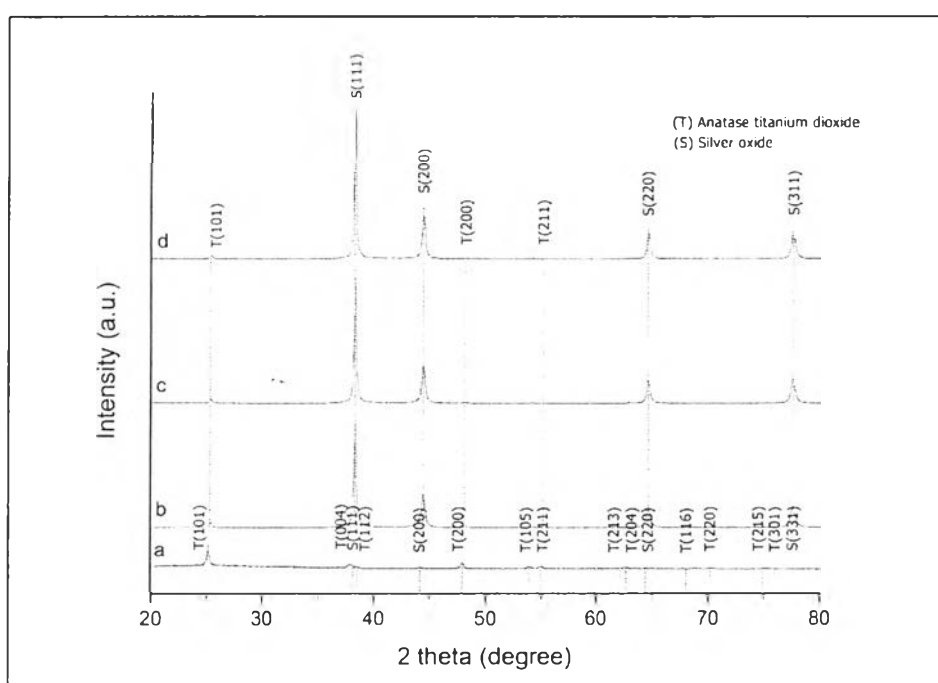


Figure 4.27 XRD patterns of (a) Ag/TiO_2 composite hollow fibers which acquired after calcination and $\text{Ag}_2\text{O}-\text{TiO}_2$ composite hollow fibers obtained after hydrothermal treatment for 1 h at (b) 110 °C, (c) 115 °C, and (d) 120 °C.

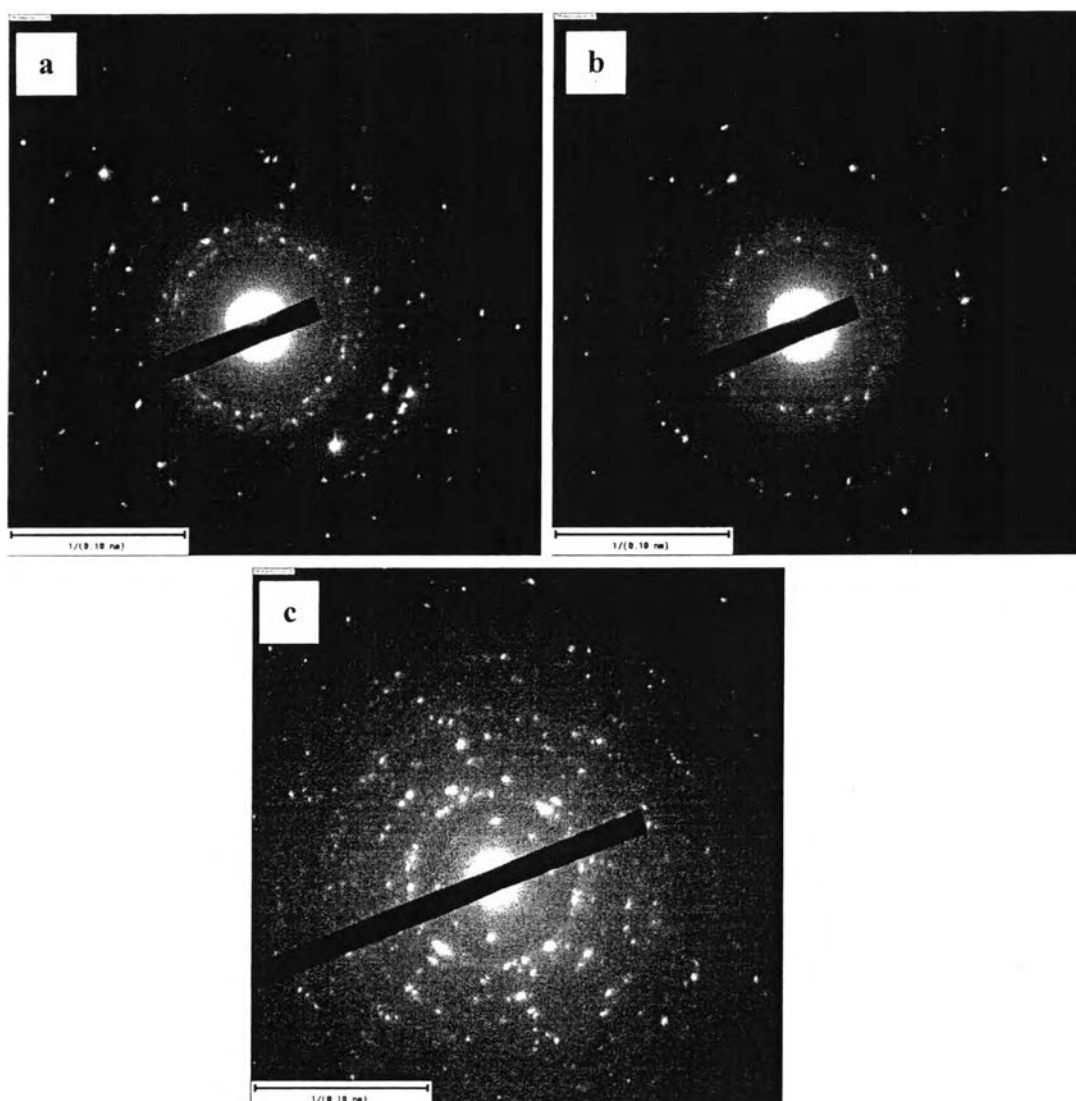


Figure 4.28 SAED patterns of $\text{Ag}_2\text{O-TiO}_2$ composite hollow fibers acquired after hydrothermal treatment for 1 h at (a) 110 °C, (b) 115 °C, and (c) 120 °C.

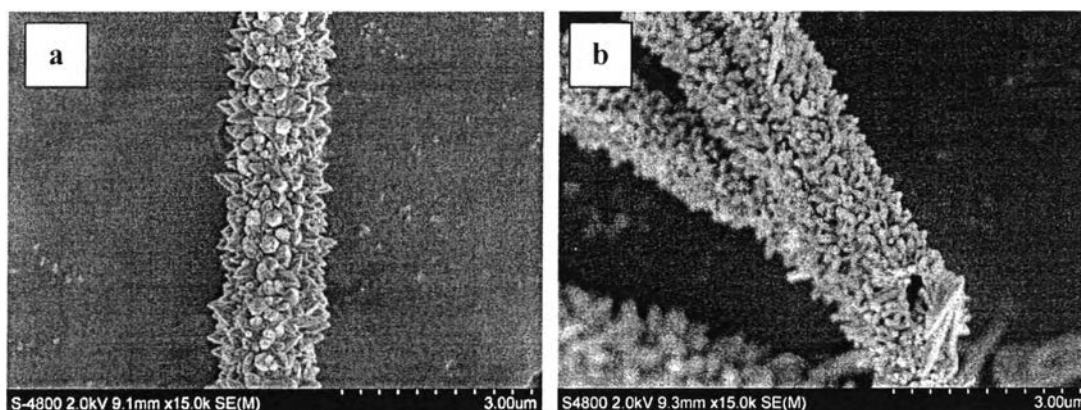
Table 4.16 The crystallite size of Ag_2O outgrowths at various temperatures

Temperature (°C)	Crystallite size (nm)
110	285.23
115	322.25
120	346.42

4.3.2 Adjusting the Hydrothermal Treatment Condition under the Fixed Temperature at 115 °C at Various Times

4.3.2.1 ZnO Outgrowths

In order to study the effect of time on the growing of ZnO branches, the calcined Zn/TiO₂ composite hollow fibers were allowed to outgrow ZnO crystals by hydrothermal treatment at 115 °C for 0.5 h, 0.75 h and 1 h. SEM images of fibers after hydrothermal treatment were illustrated in Figure 4.29. The results show that the surfaces of TiO₂ fibers hollow were completely covered by flower-like outgrowths of ZnO with the retained hollow structure. The relationship between the average fibers diameter versus time of hydrothermal treatment and the average diameter are displayed in Figure 4.30 and Table 4.17, respectively. At this point of time, as the time went longer, the average diameter became bigger. This could be explained that the crystal growth depended on how long the time was given for the crystal to grow. However, there were insignificantly differences in the average diameter in case of 0.75 h and 1 h which their diameters gained proximity. Therefore, it signified that the growth of ZnO grains as a function of time brought about a rise in the average diameter. Growing of ZnO grains could be described as the same reasons as the effect of temperature on the crystal growth as above-mentioned. But it was noticeable point that the effect of reaction time upon the crystal growth was dominant.



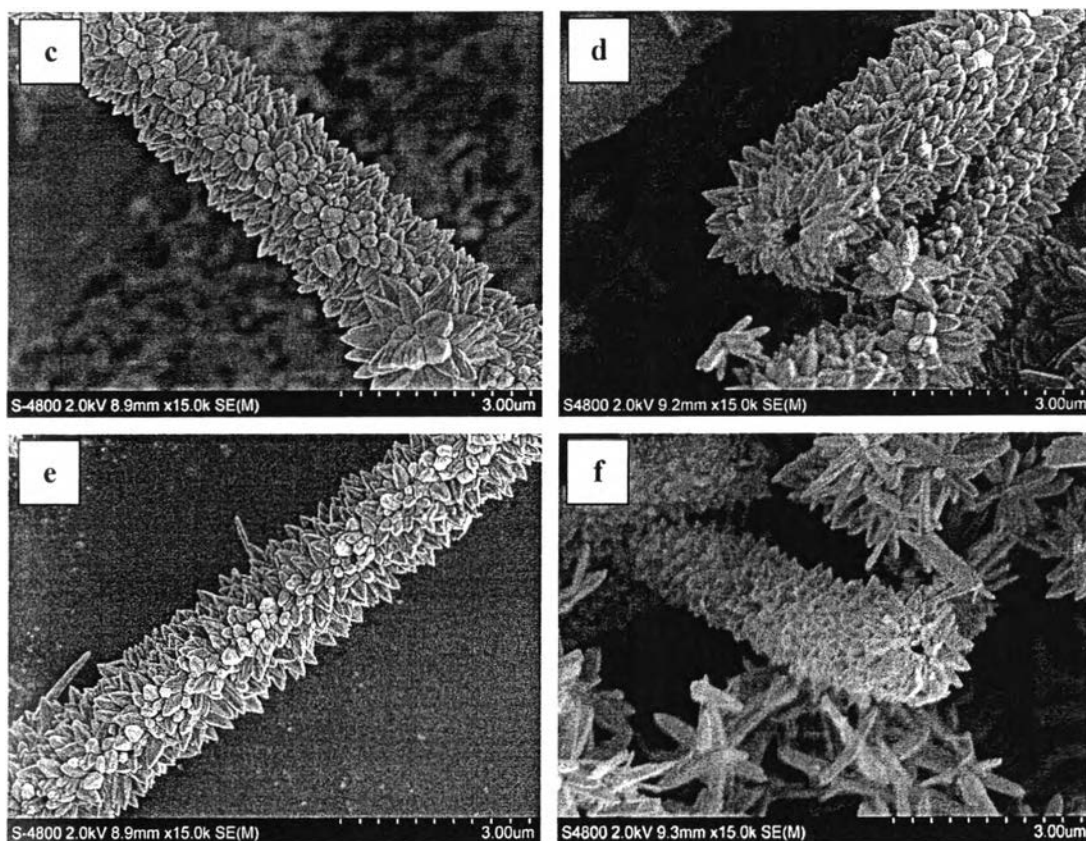


Figure 4.29 SEM images (magnification = 15000X; scale bar = 3.00 μm) of hydrothermally treated ZnO-TiO₂ composite hollow fibers at 115 °C for (a and b) 0.5 h, (c and d) 0.75 h, and (e and f) 1 h.

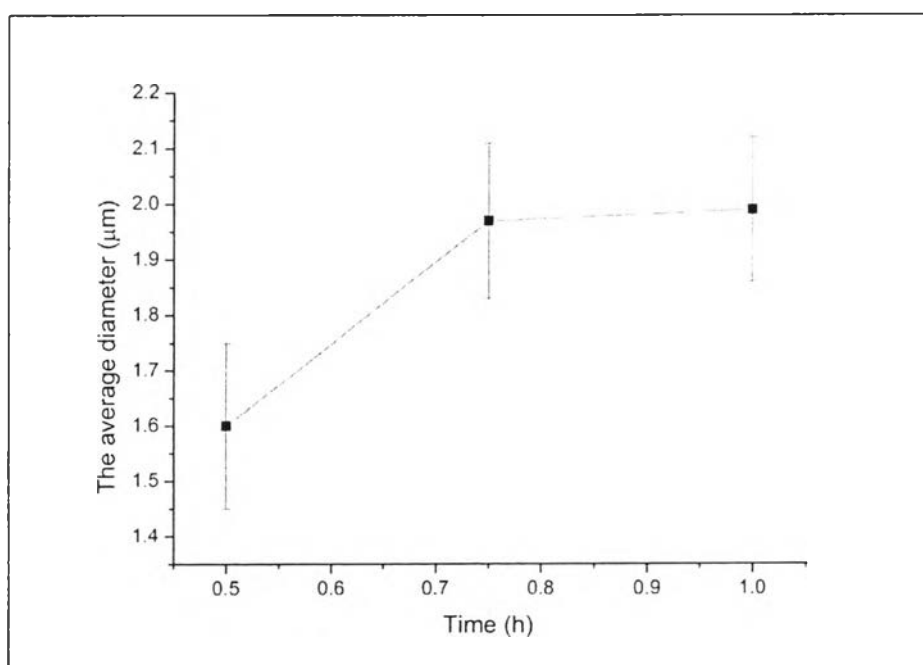


Figure 4.30 The average diameter of hydrothermally treated ZnO-TiO₂ composite hollow fibers at 115 °C as a function of time.

Table 4.17 The average diameter of ZnO-TiO₂ composite hollow fibers after hydrothermal treatment at 115 °C

Time (h)	The average diameter (μm)
0.5	1.60 ± 0.15
0.75	1.97 ± 0.14
1	1.99 ± 0.13

Besides, Figure 4.31 presents the relationship between time and weight of ZnO outgrowths obtained after hydrothermal treatment which finally became higher along with time. A rise in weight might cause from having more time to grow the crystals.

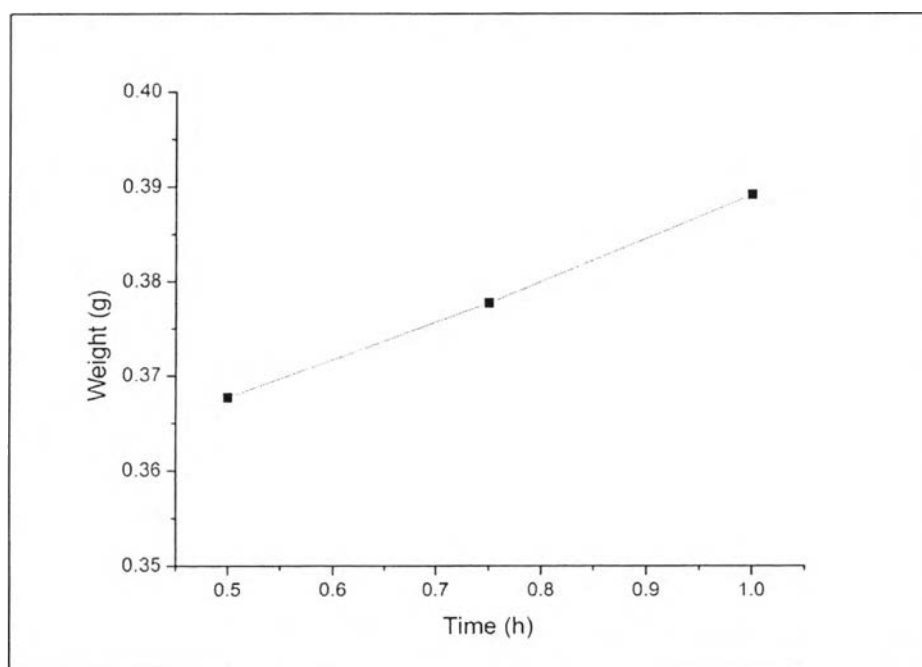
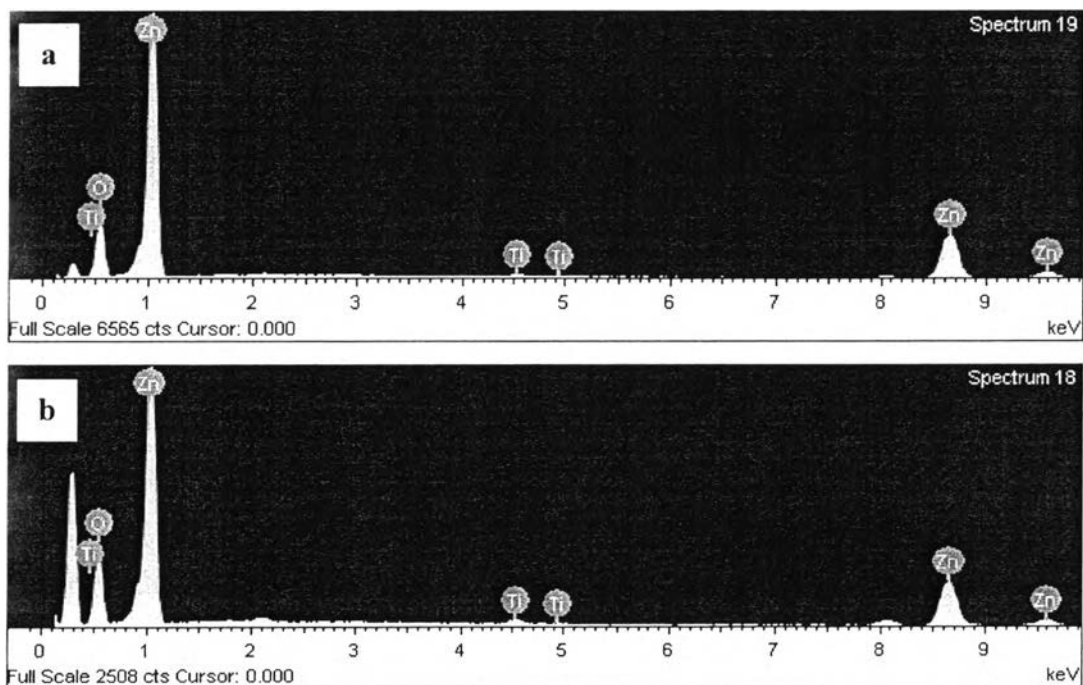


Figure 4.31 The obtained weight of ZnO outgrowths at 115 °C at different times.

Table 4.18 The weight of ZnO-TiO₂ composite hollow fibers before and after hydrothermal treatment at 115 °C

Time (h)	Weight (g)		
	before	after (without precursor)	After (with precursor)
0.5	0.0100	0.0068	0.3745
0.75	0.0100	0.0061	0.3838
1	0.0100	0.0060	0.3952

EDX results have been measured to confirm the existence of zinc oxide. At branching point, they expressed the high intensity of zinc signals accompanied with the almost absent titanium signals (see Figure 4.32(a-c)). Thus, these recommended that ZnO branches occurred from hydrothermal treatment were considered as titanium-free which are similar to the case of temperature effect.



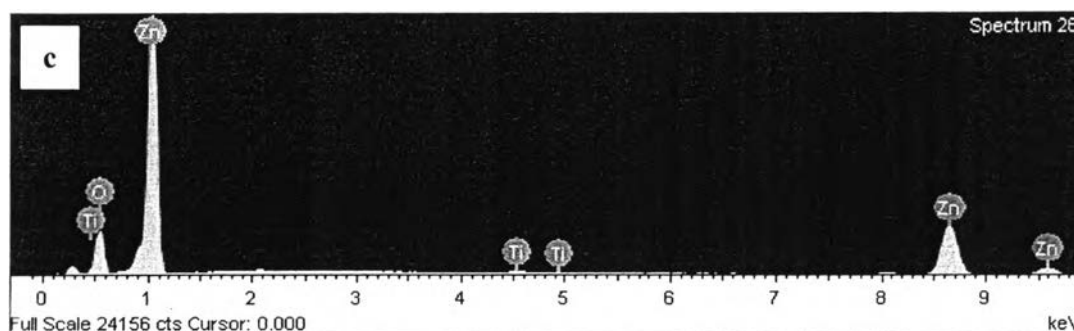


Figure 4.32 EDX results of hydrothermally treated ZnO-TiO₂ composite hollow fibers at 115 °C for (a) 0.5 h, (b) 0.75 h, and (c) 1 h.

Table 4.19 The atomic percentage of hydrothermally treated ZnO-TiO₂ composite hollow fibers at 115 °C at various times

Atomic (%)	Time (h)								
	0.5			0.75			1		
	O	Ti	Zn	O	Ti	Zn	O	Ti	Zn
	53.20	2.25	44.55	44.35	2.68	52.97	48.46	2.75	48.79

The typical XRD patterns of Zn/TiO₂ composite hollow fibers obtained after calcination and ZnO-TiO₂ composite hollow fibers obtained after hydrothermal treatment at 115 °C for 0.5 h, 0.75 h and 1 h are investigated in Figure 4.33. Pattern (a) reveals the crystalline peaks at 2θ degree of 25.35°, 37.951°, 48.092°, 54.089°, 55.135°, 70.314°, and 75.153° with respect to the crystal planes of (101), (004), (200), (105), (211), (220), and (215) (JCPDS card No 21-1272). This pattern of the calcined Zn/TiO₂ composite hollow fibers is surely indicated that the anatase phase of titanium oxide has been formed as the mention before. For the pattern (b-d), some peaks could be found as the new peaks appeared after the hydrothermal treatment process which indicated that the produced ZnO was monophasic zincite with a hexagonal structure (JCPDS card No 36-1451). These apparent peaks proved the formation of zinc oxide after undergoing hydrothermal treatment. Even though, new peaks were created, the peak with regard to anatase titanium oxide could be seen in these three patterns. In addition, the crystallite size of

ZnO outgrowths after hydrothermal treatment at various times were calculated by the Scherrer's equation of the peaks regarding to ZnO which correspond to the crystal plane of (101) and displayed in Table 4.20. From the results, the crystallite size became bigger as the time went longer.

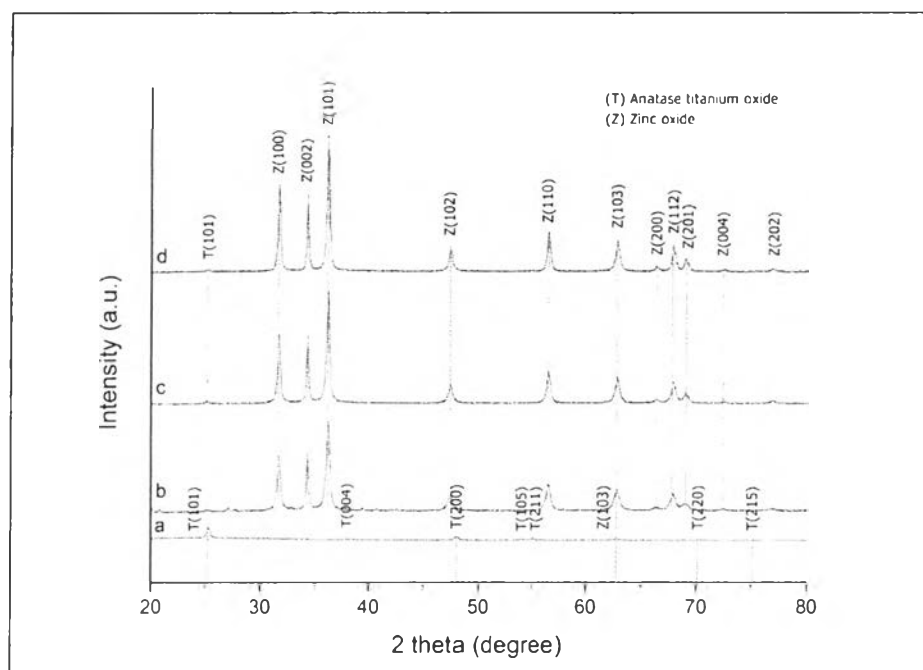


Figure 4.33 XRD patterns of (a) Zn/TiO₂ composite hollow fibers obtained after calcination and ZnO-TiO₂ composite hollow fibers obtained after hydrothermal treatment at 115 °C for (b) 0.5 h, (c) 0.75 h, and (d) 1 h.

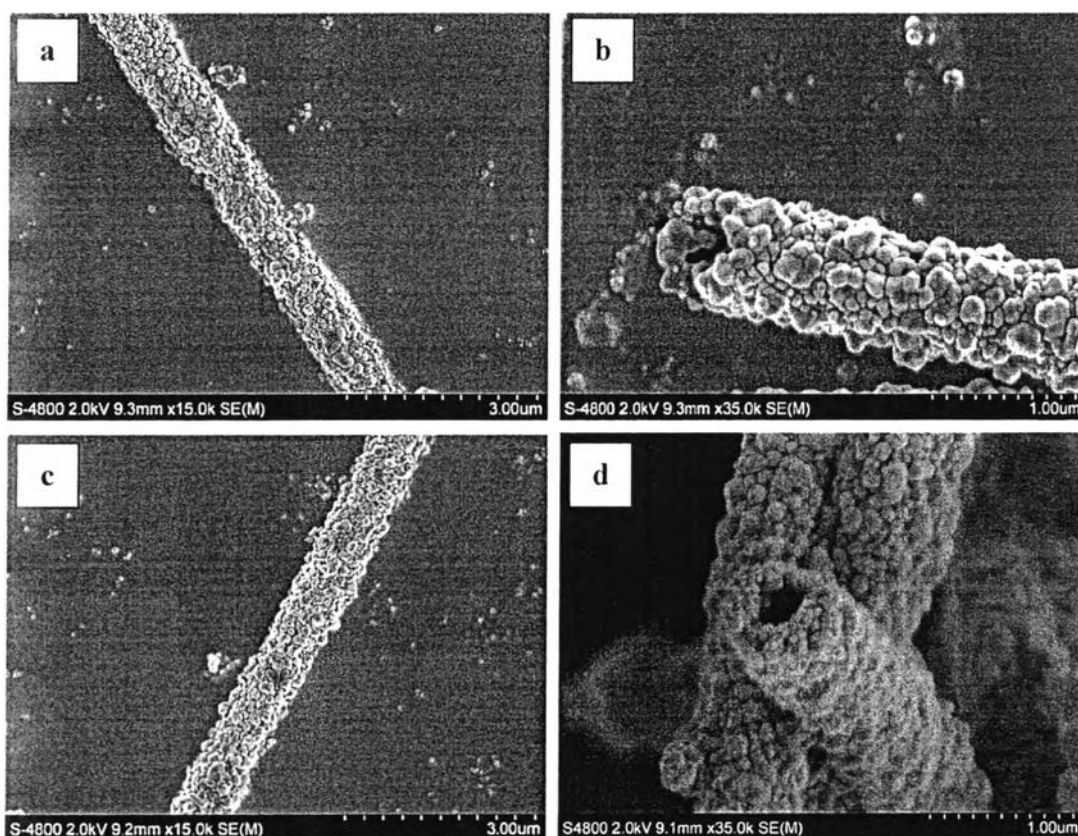
Table 4.20 The crystallite size of ZnO outgrowths at various times

Time (h)	Crystallite size (nm)
0.5	229.51
0.75	270.90
1	286.86

4.3.2.2 Ag₂O Outgrowths

The effect of time on the growth of Ag₂O crystals on TiO₂ fiber surface has been studied as well. The hydrothermal treatment was employed to

use in the process which the calcined Ag/TiO₂ composite hollow fibers were operated at 115 °C for 0.5 h, 0.75 h and 1 h. Added Ag metals were exploited as seeds to start the growth. The final products got cubic-like outgrowths growing all over the surface of TiO₂ fibers and hollow structures could be obviously seen (see in Figure 4.34 of SEM images). The average fibers diameter as a function of time were also observed in Figure 4.35. The number of nucleation sites available relied on time which eventually brought about an increasing in a number of crystal growths. These denoted that an increasing in diameter was allowed to get sufficient time to create the growth. The reason for growing out of Ag₂O grains has been already explained as aforesaid. Nevertheless, the average diameter slightly increased as a function of time. It could be said there was no significant dissimilarity.



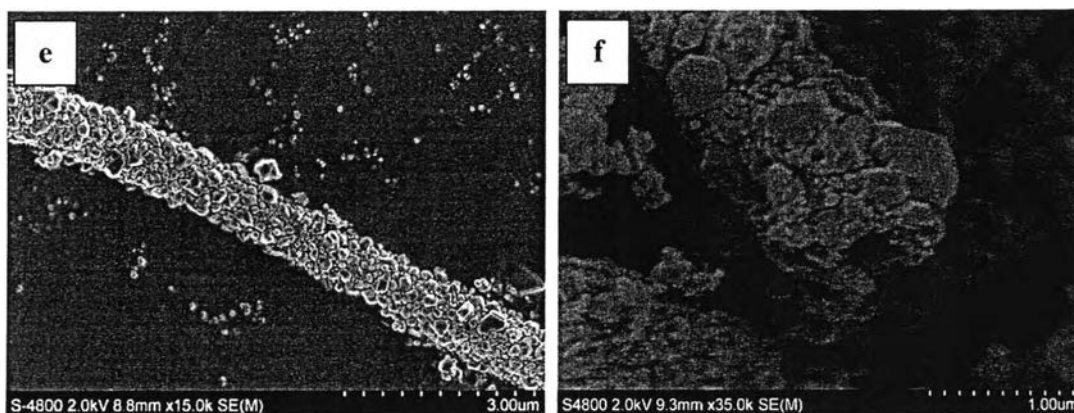


Figure 4.34 SEM images of hydrothermally treated $\text{Ag}_2\text{O-TiO}_2$ composite hollow fibers at 115°C for (a) 0.5 h, (c) 0.75 h, and (e) 1 h at magnification = 15000X; scale bar = $3.00\ \mu\text{m}$ and for (b) 0.5 h, (d) 0.75 h, and (f) 1 h at magnification = 35000X; scale bar = $1.00\ \mu\text{m}$.

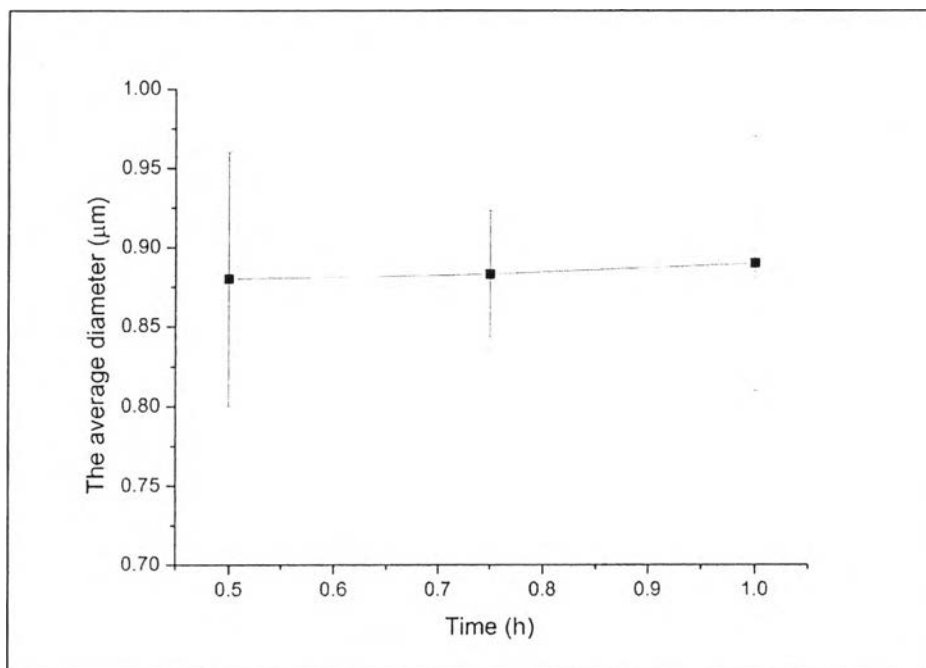


Figure 4.35 The average diameter of hydrothermally treated $\text{Ag}_2\text{O-TiO}_2$ composite hollow fibers at 115°C as a function of time.

Table 4.21 The average diameter of Ag₂O-TiO₂ composite hollow fibers after hydrothermal treatment for 1 h

Time (h)	The average diameter (μm)
0.5	0.880 ± 0.08
0.75	0.883 ± 0.04
1	0.890 ± 0.08

The relationship between time and weight of Ag₂O obtained after hydrothermal treatment process is demonstrated in Figure 4.36. The weight increased with increasing time due to the higher amount of crystals. This exhibited unidirectional result as the case of ZnO outgrowths. The weight of materials of both the pre-hydrothermal treatment and hydrothermally treated ones are also showed in Table 4.22.

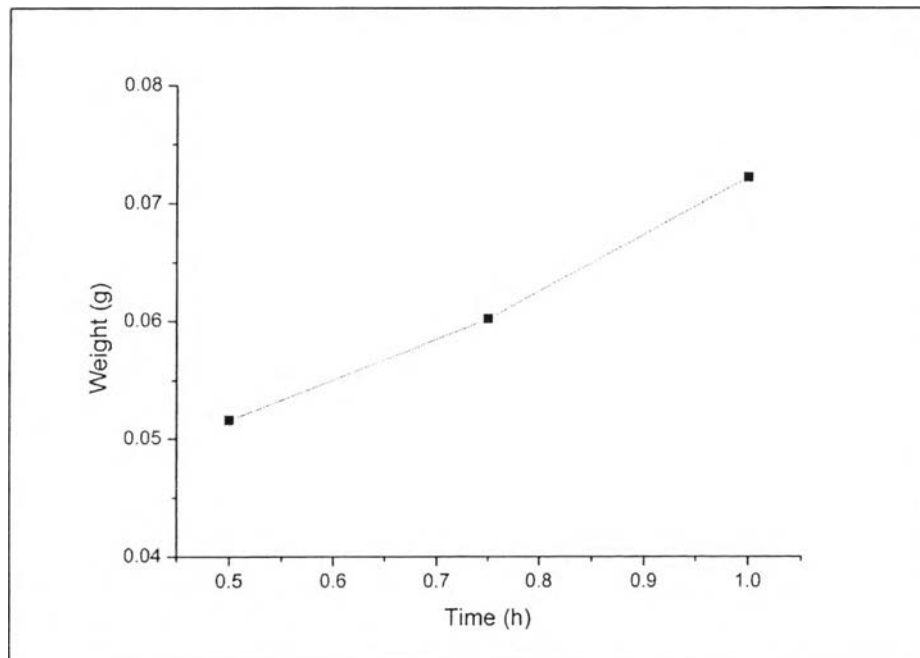
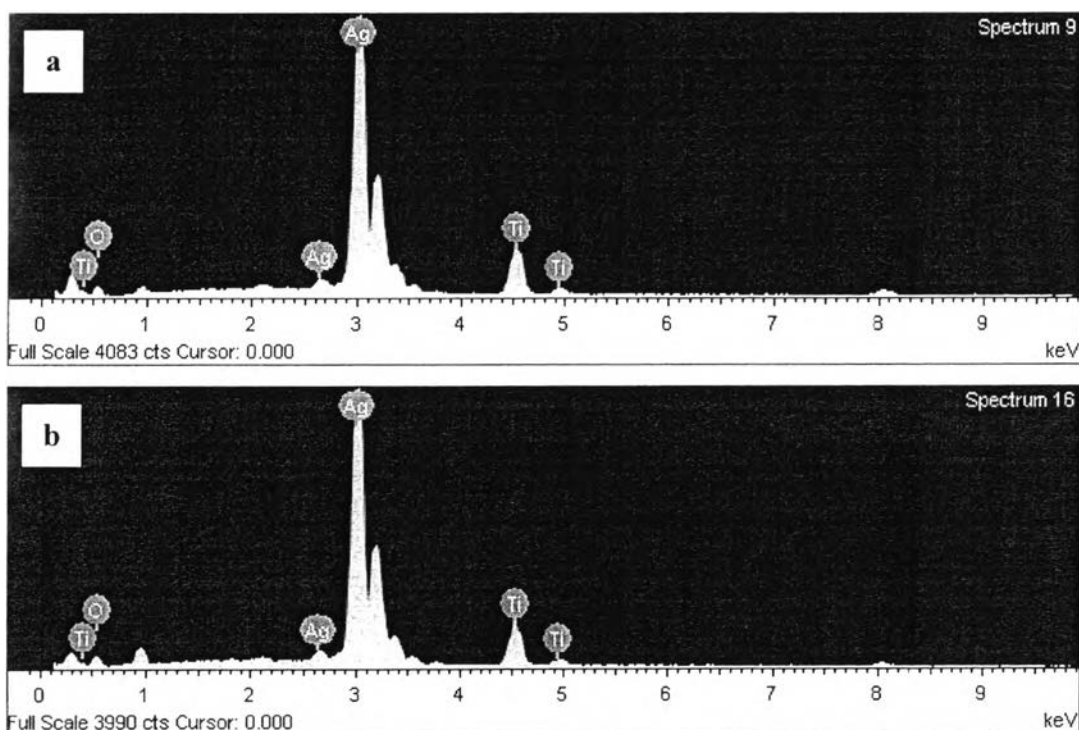


Figure 4.36 The obtained weight of Ag₂O outgrowths at 115 °C as a function of time.

Table 4.22 The weight of Ag₂O-TiO₂ composite hollow fibers before and after hydrothermal treatment at 115 °C

Time (h)	Weight (g)		
	before	after (without precursor)	After (with precursor)
0.5	0.0100	0.0069	0.0585
0.75	0.0100	0.0058	0.0660
1	0.0100	0.0060	0.0782

Moreover, Figure 4.37 represents the EDX results for outgrowing parts produced by hydrothermal treatment at various times. The analysis had been performed the high intensity of silver that signified the product obtained after hydrothermal treatment composed of a maximum silver content. Therefore, this finding should be assumed that Ag₂O outgrowing parts were able to be created by hydrothermal treatment.



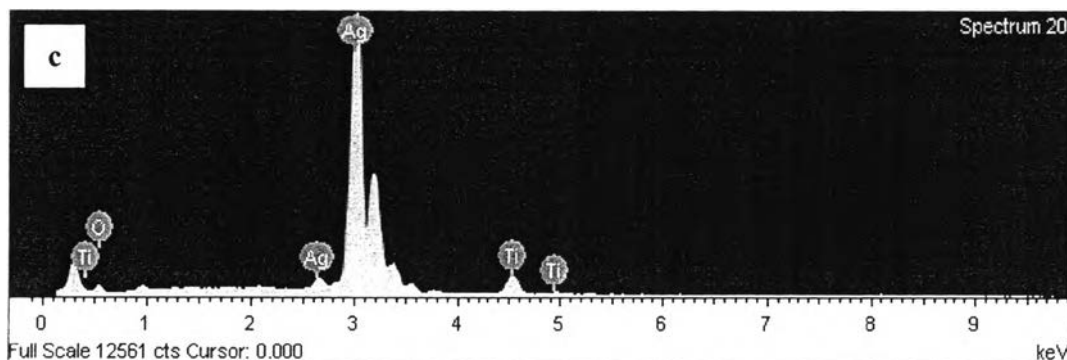


Figure 4.37 EDX results of hydrothermally treated $\text{Ag}_2\text{O-TiO}_2$ composite hollow fibers at 115 °C for (a) 0.5 h, (b) 0.75 h, and (c) 1 h.

Table 4.23 The atomic percentage of hydrothermally treated $\text{Ag}_2\text{O-TiO}_2$ composite hollow fibers at 115 °C at various times

Atomic (%)	Time (h)								
	0.5			0.75			1		
	O	Ti	Ag	O	Ti	Ag	O	Ti	Ag
	15.78	20.56	63.67	14.83	22.96	62.22	11.54	12.96	75.50

XRD patterns of Ag/TiO_2 composite hollow fibers after undergoing calcination and $\text{Ag}_2\text{O-TiO}_2$ composite hollow fibers after hydrothermal treatment at 115 °C for 0.5 h, 0.75 h and 1 h are explored in Figure 4.38. As the results shown in the pattern (a) the crystalline peaks of the anatase phase of titanium oxide had been found at 2θ degree of 25.211°, 37.771°, 38.427°, 47.947°, 53.874°, 54.993°, 62.105°, 62.666°, 68.752°, 70.191°, 75.208° and 76.039° corresponding to the crystal planes of (101), (004), (112), (200), (105), (211), (213), (204), (116), (220), (215), and (311) (JCPDS card No 21-1272). These are able to be confirmed that anatase phase of TiO_2 completely formed and other phases absolutely disappeared. In addition, in the pattern (a), at 2θ degree of 37.991°, 44.14°, 64.372°, and 77.301° corresponded to the crystal planes of (111), (200), (220), and (311) of 3C silver with a cubic crystal structure. The discovered peaks could be explained as coming from dispersed nanoparticles of silver metals which added in the precursor

before electrospinning process. These results were in accord with EDX results. In case of XRD pattern (b-d), after the hydrothermal treatment process for 0.5 h, 0.75 h and 1 h, the peaks with regard to Ag_2O treatment (JCPDS card No 04-0783) increased in intensity which are supposed to be the results from hydrothermal treatment. A rise in intensity suggested that the products got higher crystallinity. The hydrothermal treatment occurred, however, some peaks with respect to anatase titanium oxide still be remained. Besides, the crystallite size of Ag_2O outgrowths after hydrothermal treatment at various times were calculated by the Scherrer's equation and displayed in Table 4.24. According to the results, the crystallite size did not have significant difference in the size after hydrothermal treatment at various times. These supported the results of the average diameter.

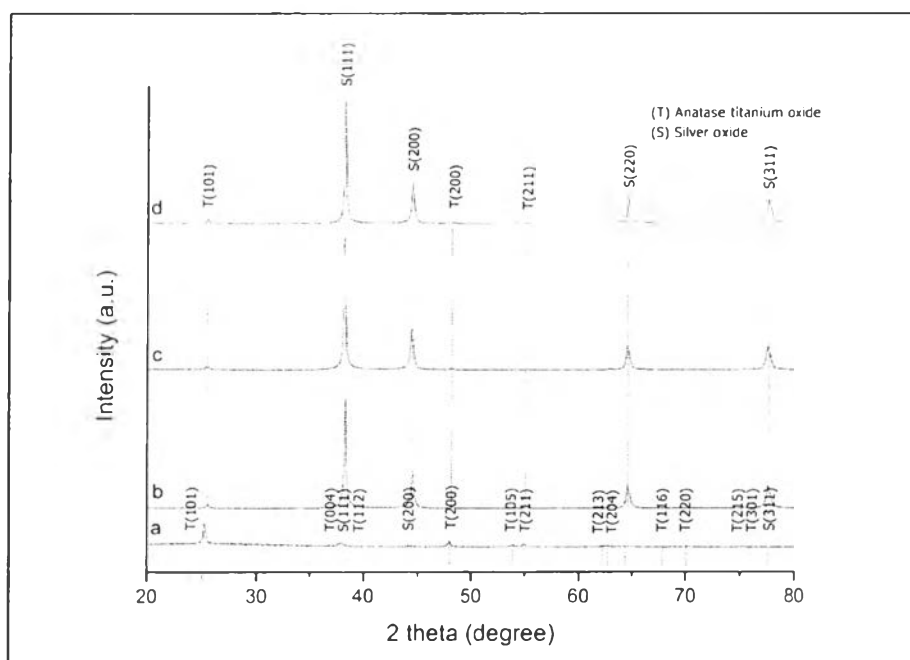


Figure 4.38 XRD patterns of (a) Ag/TiO₂ composite hollow fibers acquired after calcination and Ag₂O-TiO₂ composite hollow fibers obtained after hydrothermal treatment at 115 °C for (b) 0.5 h, (c) 0.75 h, and (d) 1 h.

Table 4.24 The crystallite size of Ag₂O outgrowths at various times

Time (h)	Crystallite size (nm)
0.5	323.54
0.75	323.43
1	322.25

More details of the BET values were presented in Table 4.25. In general, BET theory is used to explain the physical adsorption of gas molecules on a solid surface. Adsorption is defined as the adhesion of atoms or molecules of gas to a surface. The amount of gas adsorbed, typically called adsorbate, not only depends on the exposed surface but also on the temperature, gas pressure and strength of interaction between the gas and solid surface. Whenever solid matter is cut into smaller particles, new surfaces are created which results in increasing the surface area. Similar to the created pores within the particle interior either by dissolution, decomposition or some other physical or chemical methods, the surface area is accrued as well. According to the results, TiO₂ hollow fibers provided the surface area (39.072 m²g⁻¹) higher than the value obtained from TiO₂ fibers. This can be assumed the unique structure of hollow fibers is capable of enhancement of surface area. As considering to the effect on temperature on the surface area attained after hydrothermal treatment of ZnO-TiO₂ composite hollow fibers of all conditions, BET surface area tended to decrease substantially compared to pre-hydrothermally treated one. Similarly, BET surface area slightly reduced with the longer time, approximately from 25 down to 13 m²g⁻¹ (temperature fixed at 115 °C). These results contrasted with the basic principle of BET method that if solid matter is divided into smaller particles, new surfaces are created which finally lead to a rise in the surface area. It probably occurred due to either the migration of material from smaller size to larger one or the collapse of pore structure collaborated with the crystallite growth at the higher time and temperature. According to the temperature effect results on the surface area of the Ag₂O-TiO₂ composite hollow fibers, BET surface area decreased across the temperature range, from 44 down to 13 m²g⁻¹. This loss in surface area was presumably associated with a significant decrease in the pore structure.

Nonetheless, Ti₂O-based fibrous materials will promote the high capacity owing to the stable phase of anatase TiO₂ which commonly provides lithium storage sites. Furthermore, the hollow interior was believed to have ability to utilize as anode materials as the following reasons. First, this structure can endow the extra free-space to store lithium ion and alleviate the volume variation associated with lithiation/delithiation during cycling, resulting in improvement of cycle stability. Second, it is able to reduce path length in the solid state diffusion of anode materials for both of lithium ion and electron, giving better rate capability (Lui *et al.*, 2010 and Wang *et al.*, 2012). In fact, high surface area anode materials usually provide large contact area between electrode and electrolyte electrode-electrolyte, leading to great development of rapid charging and discharging as well as reaction kinetics. Even though, the surface modification of both types of composite hollow fibers in this work could not give satisfactory results of surface area obtained after modification, the changing in the surface structure was of great prominence to its stability. The anode materials normally suffer from the drawbacks due to the inevitably attack by electrolyte which considerably extend the process of lithiation/delithiation. This is well suppressed by the ZnO and Ag₂O outgrowths which were capably attached on the surface of TiO₂ hollow fibers. These surface modified can efficiently cure not only the disintegration/pulverization of anode but also the decomposition of electrolyte accompanied with electrode. As a result of significant mitigation, the modified materials thus furnish high stability (Kanjwal *et al.*, 2010).

Table 4.25 BET surface area of the obtained materials

Materials	BET surface area (m^2g^{-1})
TiO ₂ fibers	30.812
TiO ₂ hollow fibers	39.072
Pre-hydrothermally treated ZnO-TiO ₂ composite hollow fibers	52.351
ZnO-TiO ₂ (110 °C 1 h)	N/A
ZnO-TiO ₂ (115 °C 1 h)	19.440
ZnO-TiO ₂ (120 °C 1 h)	N/A
ZnO-TiO ₂ (115 °C 0.75 h)	22.760
ZnO-TiO ₂ (115 °C 0.5 h)	25.164
Pre-hydrothermally treated Ag ₂ O -TiO ₂ composite hollow fibers	36.724
Ag ₂ O -TiO ₂ (110 °C 1 h)	44.960
Ag ₂ O -TiO ₂ (115 °C 1 h)	39.510
Ag ₂ O -TiO ₂ (120 °C 1 h)	13.387
Ag ₂ O -TiO ₂ (115 °C 0.75 h)	N/A
Ag ₂ O-TiO ₂ (115 °C 0.5h)	N/A

4.4 Lithium Ion Battery Study

The charge-discharge characteristic of the cells was studied as well. The prepared electrodes (anode and cathode) showed the geometrical area of 1.0 cm^2 with a thickness of $\sim 10 \text{ }\mu\text{m}$. They had a smooth and homogeneous surface with the appearance of black color. Figure 4.38 showed the digital photos of the prepared anode, cathode, and separator (the geometrical area = 1.5 cm^2 , thickness = 1 mm).

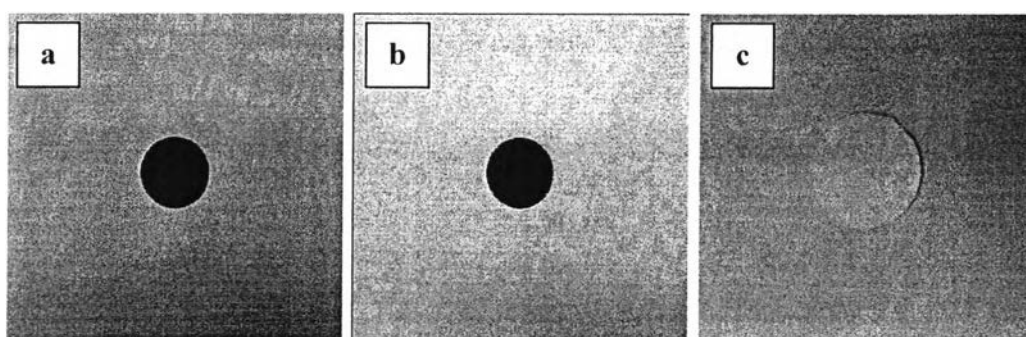


Figure 4.39 The digital photos of the prepared (a) anode, (b) cathode, and (c) separator.

Figure 4.40 shows the charge capacity at current density of 80 mA g^{-1} in $0.04\text{-}4 \text{ V}$ for ZnO-TiO₂ composite hollow fibers under the hydrothermally treated condition of $115 \text{ }^\circ\text{C}$ 0.5 h which provided the highest surface area approximately $25.164 \text{ m}^2\text{g}^{-1}$ compared to other conditions. It exhibited charge capacity of 443 mAhg^{-1} . On the other hand, for discharge capacity, it could not be examined. This might result from inefficient assembly of cell. Thus, it should be noted that the requirement of good packing of cell is essential in order to carry out the electrochemical characterizations.

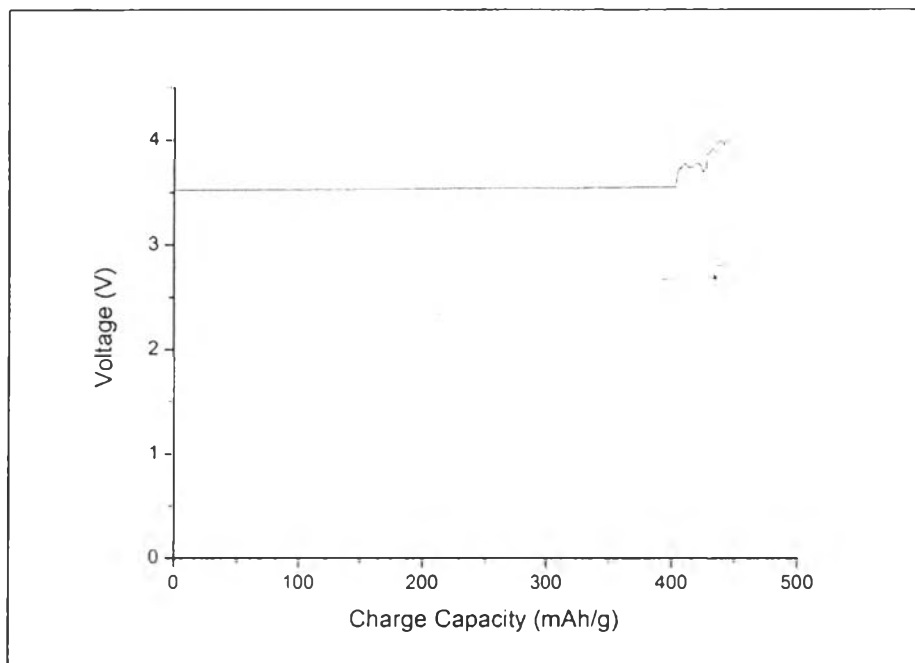


Figure 4.40 Charge curve of hydrothermally treated ZnO-TiO₂ composite hollow fibers under the condition of 115 °C 0.5 h.